



COMPUTER SCIENCE
UC SANTA BARBARA

UNIVERSITY OF CALIFORNIA, SANTA BARBARA

DEPARTMENT OF COMPUTER SCIENCE

MASTERS CANDIDATE PROJECT REPORT

Metabolomics Techniques and Assessment of Acute Kidney Injury on Distant Organ Function

Supervisor:

Dr. Linda Petzold

Author:

Ben Fox

b_fox@ucsb.edu

(719) 338-4628

Committee Member:

Dr. Xifeng Yan

Corresponding Supervisor:

Dr. Sarah Faubel
CU Denver Medical Campus

June 6, 2019

Contents

1	Introduction	2
1.1	Metabolomics	2
1.2	AKI	3
1.3	Present study	4
2	Materials and Methods	4
2.1	Animals	4
2.2	Surgical protocol	4
2.3	Experimental groups and accounting for mice included in experiments and analysis	5
2.4	Collection and preparation of plasma, heart, kidney, liver, lung samples	5
2.5	Metabolomics sample preparation, data collection, and metabolomics data overview	5
2.6	Heart and lung ATP assays	6
3	Metabolomics Techniques and Statistical Analyses	6
3.1	Overview	6
3.2	Metabolomics Data Pre-processing	6
3.3	$P >> N$ problem	7
3.4	Univariate methods	8
3.5	Unsupervised methods	8
3.5.1	Hierarchical clustering analysis	9
3.5.2	Principal component analysis	9
3.6	Supervised methods	10
3.6.1	Partial least squares discriminant analysis	10
3.7	Pathway enrichment analysis	13
3.7.1	Pathway activity profiling	14
3.7.2	Metabolite set enrichment analysis	14
4	Results and Discussion	15
4.1	Time course of AKI	15
4.2	AKI and distant organ effects	16
4.2.1	Significant metabolites	16
4.2.2	Specific metabolites and metabolic pathways affected in distant organs by AKI	17
4.2.3	ATP levels in the heart and lung	18
4.2.4	Amino acid deficiencies	18

4.2.5	Alternative energy metabolism	20
4.2.6	Oxidative stress	21
4.3	Overall implications	22
5	Concluding Remarks and Limitations	23
6	Supplementary Material	31
6.1	HCA	31
6.2	PCA	36
6.3	Effect of AKI metabolites	41
6.4	PAPi HCA	48
6.5	Enriched pathways significant to AKI	53
6.6	Box and whisker plots	55
6.6.1	Amino acids in the heart	55
6.6.2	Amino acids in the lung and liver	56
6.6.3	Glycolysis/TCA Cycle/Pentose Phosphate Pathway	56
6.6.4	Purine and pyrimidine metabolism	59
6.6.5	Oxidative stress	61
6.7	Metabolites with the highest cosine similarity metrics in PCA	63
6.8	Metabolites with the highest PLS-DA weights	68

Abstract

Metabolomics is the large scale study of small organic molecules (metabolites) within an organism, tissue, or cell. This technique and its application to systemic diseases is revealing of potential diagnoses and treatments offering a significant advancement to the medical and clinical communities. However, statistical methods for metabolomics are often misunderstood due to low sample sizes and large feature sets and interpretability of experimental results is difficult without established knowledge of biochemistry and the disease domain. This paper aims to elaborate the statistical techniques utilized in metabolomics as well as apply them to a widespread systemic disease, acute kidney injury (AKI), to better understand the disease state. AKI is associated with widespread effects on distant organs, including the heart, lung, and liver, and is incident in upwards of 20% of hospitalized patients and 70% of intensive care unit patients. In this study, metabolomics analysis was performed on five separate organ tissues to examine the effect of AKI on distant organs in mice, under the hypothesis that AKI would have deleterious effects on distant organs, specifically the heart, lung, and liver and cause shifts from oxidative phosphorylation generation of ATP to alternative energy metabolism and oxidative stress. Metabolomics statistical techniques were utilized to identify metabolites and biochemical pathways associated with organ dysfunction in AKI, and build classifiers to predict onset of AKI. In total, 43%, 21%, and 33% of metabolites measured were affected at some time point after AKI in the heart, lung, and liver respectively. Additionally, a plasma PLS-DA classifier was built with 98.46% accuracy and could be utilized to assist doctors in diagnosis of early onset of AKI. This study demonstrates that AKI is associated with dramatic changes in heart, lung, and liver metabolism, ATP depletion, and oxidative stress, with the most dramatic effects in the heart. Treatment methods for AKI should be explored further specifically focused on amino acid and antioxidant supplementation and examining the role of glucose and other sugars and starches post AKI.

1 Introduction

1.1 Metabolomics

Metabolomics is the large-scale study of small organic molecules (metabolites) within an organism, tissue, or cell. Metabolites are defined as molecules that are less than 1,500 Daltons (or atomic mass units; 1 Dalton \approx 1 hydrogen atom in mass). Identification of metabolites in an organism, tissue, or cell is typically performed via mass spectrometry (MS) or nuclear magnetic resonance (NMR), after processing a tissue or blood sample. Both methods return a spectra of peaks that are cross referenced with databases matching

spectra to metabolites. Characterization of these spectra and metabolites has been an ongoing process for the past twelve years. Similar to the human genome project, the human metabolome project began characterizing human metabolites in 2007. Initially, around 3,000 metabolites were identified in the human body [1]; however, that number has risen substantially to 114,000 in 2018 [2]. This number is expected to continue to grow as methods of identification (MS/NMR) become more precise. Some examples of metabolites include amino acids, sugars, fatty acids, lipids, and more. Metabolomics is closely related to other types of “omics” techniques such as genomics, transcriptomics, and proteomics. For context, genomics is the large-scale study of genes, transcriptomics is the large-scale study of mRNA, and proteomics is the large-scale study of proteins. Metabolomics is a more powerful approach compared to these methods because metabolites and their concentrations are a direct reflection of the biochemical activity and state of a cell, tissue, or organism, thus revealing a phenotypic state. This state is affected by internal mechanisms (genes, mRNA, and proteins) in addition to the external environment. In other words, metabolomics is a direct representation of what is currently occurring in a cell, tissue, or organism. As a quick example, let’s examine the metabolite glucose. Glucose levels in the blood are affected by the external environment via an organism’s sugar intake from food. Internally, they’re affected by how much insulin (which causes re-uptake of glucose into cells) the pancreas produces, which is controlled by a variety of genes, mRNA, and proteins. In diabetes, the knowledge of these metabolic interactions are taken advantage of by having a patient inject insulin to change the state of the metabolite glucose. With this in mind, it becomes clear that in any disease state, metabolomics can offer insight to diagnose (by identifying significant metabolites and pathways) and treat diseases (by further studies to mediate such changes in the metabolome). Thus, metabolomics has vast potential for the biological and medical communities.

1.2 AKI

Acute kidney injury (AKI) is a common complication, with an incidence of 3% to 20% in hospitalized patients and 22% to 67% in intensive care unit (ICU) patients [3]. Further, the incidence of AKI in recent years in hospitalized patients has increased 11% annually [4]. Supportive treatment for severe AKI is renal replacement therapy (RRT), which includes dialysis, and is based on the removal of damaging substrates in the blood. In terms of mortality, approximately 2 million people who develop AKI die each year. AKI has been shown to have varying mortality rates, ranging from 11.6% in one study [3] to 33.7% in another [5] for hospitalized patients after 90 days. Mortality rates amongst critically ill (ICU) patients ranged from 40-70% [6, 7]. AKI itself is associated with increased mortality rates in patients [8, 9]. Clinical and basic research into the mechanisms by which AKI

leads to increased mortality has revealed that AKI is a systemic disease with widespread, deleterious effects on distant organs, including the heart, lung, and liver [10, 11, 12, 13]. While it is known that AKI has detrimental effects on distant organs, metabolomics analyses have not been performed.

1.3 Present study

In this paper, metabolomics statistical techniques are overviewed and these techniques are applied to a metabolomics analysis performed on the heart, lung, liver, kidney, and plasma tissue at 4 hours, 24 hours, and 7 days after ischemic AKI was administered to mice to test the hypothesis that the distant organ metabolomes (heart, lung, and liver) would be characterized by impaired oxidative phosphorylation, increased oxidative stress, and evidence of alternative energy production. This study is the first of its kind to examine the metabolome of these distant organs after AKI.

2 Materials and Methods

2.1 Animals

Adult (8-10 week old), male C57BL/6 mice (Jackson Laboratories, Bar Harbor, ME) weighing between 20-25 g were used. Mice were maintained on a standard diet, and water was freely available. All experiments were conducted with adherence to the National Institutes of Health Guide for the Care and Use of Laboratory Animals. The animal protocol was approved by the Animal Care and Use Committee of the University of Colorado, Denver.

2.2 Surgical protocol

Two surgical procedures were performed: (1) sham operation (i.e., laparotomy - surgical incision into the abdominal cavity) and (2) ischemic AKI. For all procedures, mice were anesthetized with intraperitoneal avertin (2,2,2 tribromoethanol; Sigma Aldrich, Milwaukee, WI) and a laparotomy was performed. In the ischemic AKI group, both renal pedicles were clamped for 22 minutes. Mice received 500 μ l saline with buprenex subcutaneous injection prior to surgery; 500 μ l saline was administered by subcutaneous injection every day after surgery. Sham operation consisted of the same procedure except that clamps were not applied.

2.3 Experimental groups and accounting for mice included in experiments and analysis

The study began with 10 mice per group for each of the 7 experimental groups: 1) normal (no surgical procedure), 2) 4 hour sham, 3) 4 hour AKI, 4) 24 hour sham, 5) 24 hour AKI, 6) 7 day sham, and 7) 7 day AKI for a total of 70 mice. However, 1 mouse in the 7-day sham group died, and 4 mice in the 7-day AKI group died. Thus, the numbers of animals included in the final data analysis are as follows: 1) normal: n=10, 2) 4 hour sham: n=10, 3) 4 hour AKI: n=10, 4) 24 hour sham: n=10, 5) 24 hour AKI: n=10, 6) 7 day sham: n=9, and 7) 7 day AKI: n=6. Serum creatinine and blood urea nitrogen (BUN) were measured to confirm onset of AKI. Both measures are widely utilized diagnoses standards for AKI.

2.4 Collection and preparation of plasma, heart, kidney, liver, lung samples

Blood was obtained via cardiac puncture and centrifuged at 3,000 rpm at 4°C for 10 minutes; plasma was collected and centrifuged a second time at 3,000 rpm for 1 minute. The left ventricle of the heart, the lung, liver, and left kidney were collected, weighed, snap frozen in liquid nitrogen, and then stored at –80°C.

2.5 Metabolomics sample preparation, data collection, and metabolomics data overview

Frozen heart, liver, lung and kidney samples were milled with a mortar and pestle in the presence of liquid nitrogen, then weighed to the nearest 0.1 mg and extracted in ice-cold lysis/extraction buffer at a concentration of 10 mg/mL. Samples were then agitated at 4°C for 30 min and then centrifuged at 10,000 g for 15 min at 4°C. Protein and lipid pellets were discarded, while supernatants were stored at –80°C until metabolomics analyses via ultra-high pressure liquid chromatography coupled to online mass spectrometry (UHPLC-MS) as previously reported [14]. Plasma samples were snap frozen and stored at –80°C until UHPLC-MS analysis.

343 metabolites were of interest (pre-selected from common energy metabolites and pathways) and mined from the identified peaks in the un-targeted UHPLC-MS metabolomics analysis. Metabolites were identified in each organ (124 for the heart, 132 for the lung, 177 for the kidney, 141 for the liver, and 128 for the plasma).

2.6 Heart and lung ATP assays

Pre-weighed murine heart left ventricle (LV) (from a separate cohort of mice) and lung tissue were processed for determination of myocardial and pulmonary ATP content using commercially available reagents as per manufacturer's instructions (Abcam; ab833355). Briefly, flash-frozen LV and lung tissue was homogenized in ATP assay buffer using Dounce homogenizer. The lysate was centrifuged at 13,000g at 4°C, and supernatant subjected to deproteinization procedure via TCA precipitation (Abcam; ab204708). The deproteinized samples were incubated with necessary reaction components for 30 minutes at room temperature protected from light. Fluorescence signals from samples were then measured on a microplate reader at Ex/Em = 535/587 nm. Serial dilutions of ATP were used to generate a standard calibration curve. ATP concentrations were calculated from the standard curve data and normalized to corresponding tissue weight.

3 Metabolomics Techniques and Statistical Analyses

3.1 Overview

There are a wide variety of metabolomics techniques. Generally, the field of metabolomics has a lot of moving parts, from actual laboratory experiments, to mass spectrometry, to spectra preprocessing and metabolite identification, to statistical analysis, and finally to interpretation of results via knowledge of biochemical pathways and individual metabolites. A wide domain of knowledge is necessary to understand all of these concepts, and this section aims to specifically elaborate post metabolomics data collection statistical analysis techniques in depth and their application to this study.

3.2 Metabolomics Data Pre-processing

After metabolites have been identified from mass spectrometry (where extensive spectra pre-processing is also done [14]), the raw data is in the form of an $n \times p$ data matrix with n samples and p metabolites and each corresponding matrix element containing a concentration or peak intensity value from the NMR or MS spectra. The next step in the metabolomics workflow for statistical analysis is to first remove missing values and normalize and scale the metabolite data for further statistical analysis. There are a variety of methods to do this, namely mean value, small value, median value, random forest, and k nearest neighbors (kNN) imputation. In this study, missing values were replaced using the kNN algorithm, with $k = 5$, identifying the five nearest samples to the sample with missing values, and imputing the average of their values for the corresponding missing value.

This has been found to perform well across un-targeted metabolomics experiments [15]. In metabolomics data, missing values are missing for three primary reasons: the metabolite concentration was above or below the limit of detection, metabolite is not present in the biological sample, or the metabolites peak was masked due to interaction with other metabolites. For single samples with missing values for metabolites, kNN imputation makes sense assuming samples nearby had measurements for the missing metabolite. Following imputation, normalization, scaling, and/or numerical transformation should be performed. There are a variety of common techniques to perform including normalization by sum, mean, reference sample, scaling by unit variance, range, pareto, and numerical transformation by log or cubed root. The choices of these depends on the study at hand. In this study, metabolites' raw peak areas were range scaled in order to allow for homoscedastic statistical tests [16, 17]. Range scaling metabolites is ideal for exploratory metabolomics analysis as it allows all metabolites to be favored equally and compares metabolites relative to their biological response range [16]. Range scaling performs the following for each metabolite x :

$$\tilde{x}_{ij} = \frac{x_{ij} - \bar{x}_i}{x_{i\max} - x_{i\min}} \quad (1)$$

3.3 $P >> N$ problem

Metabolomics data are not the traditional type of dataset where sample size n is equal to or greater than feature size p . In fact, metabolomics data typically results in $p \gg n$ problems, so much so that the primary goal of many statistical methods is to select features, reduce the dimensionality of the data, and generalize features via pathways. As analysis techniques become even better [2], un-targeted metabolomics experiments will likely result in thousands and tens of thousands of features for each sample, emphasizing the need for dimension reduction as the focused technique for any metabolomics study. As a note, getting more samples for metabolomics studies is often costly and difficult and acquiring samples to the point where $p \approx n$ is not feasible. A typical sample run for an un-targeted analysis on a UHPLC-MS can cost around \$500 per sample. This on top of the lab work and sample preparation beforehand make it a costly investment. Thus, the primary focus of the statistical analysis is dimension reduction and pathway identification. In this study, metabolites are individually identified as significant via univariate statistical methods and filtered based on significance. Additionally, unsupervised and supervised dimension reduction techniques are used to further find important metabolites and their trends and build a classifier model.

3.4 Univariate methods

Univariate statistical analyses methods for metabolomics data have been studied before [18]. Overall, data must closely meet basic requirements to perform common univariate methods: normality, homoscedasticity, and independence. Hence, missing value imputation and scaling of the data was performed to meet normality and homoscedastic requirements, and independence between samples was assumed. Common univariate methods in metabolomics include t-tests, fold change analyses, and ANOVA (depending on number of sample groups). In this study, ANOVA (significant threshold $p \leq 0.05$) was performed on scaled metabolite data on all organs. ANOVA was used to find metabolites across groups with significant differences of means; further, post hoc analysis was done to find the relevant groups that were significantly different from each other. The relevant groups were defined as follows: (i) Significant to AKI (Sig2AKI): at each time point for each metabolite, a significance test was done to determine if there was statistical significance between AKI and normal ($p \leq 0.05$), AKI and sham ($p \leq 0.05$), and no significance between sham and normal ($p \geq 0.05$), (ii) Intensified in AKI (IiAKI): at each time point for each metabolite, a significance test was done to determine if there was statistical significance between AKI and normal, AKI and sham, and sham and normal (directionality i.e. increase vs decrease was also taken into account here), (iii) Opposite in AKI (OppInAKI): at each time point for each metabolite, a significance test was done to determine if there was statistical significance between AKI and normal, AKI and sham, and sham and normal, with the condition that the sham and AKI group concentrations had opposite effects compared to normal, (iv) No Effect in AKI (NoEfAKI): at each time point for each metabolite, a significance test was done to determine if there was statistical significance between AKI and sham, sham and normal, and no significance between AKI and normal. Metabolites that met the conditions for these four groups were hypothesized to have some effect in AKI, whether it be a direct effect, an increased effect, an opposite effect, or an inhibitory effect. Due to the multiple testing problem, the Benjamini-Yekutieli p-value adjustment method was used to determine statistical significance for these pre-selected groups. The Benjamini-Yekutieli method has been found to allow for dependence assumptions across variables [19], which make it a desired method for metabolomics.

3.5 Unsupervised methods

Multivariate statistical analyses methods are primarily used in metabolomics data to reduce dimensionality. Additionally, they help with identifying and understanding trends across metabolites and samples, identifying sample outliers, and visualizing high dimensional spaces. The two higher level statistical categories used for multivariate analysis in metabolomics are unsupervised and supervised learning methods. The main difference

between these two types of approaches is that unsupervised learning does not consider class membership, while supervised learning does. Unsupervised learning thus provides an overview of the groups and trends in the data [20], without a knowledge of the underlying groups. There are many unsupervised learning methods that can be used for metabolomics analyses such as hierarchical clustering analysis (HCA), principal component analysis (PCA), *k*-means clustering, and self-organizing maps (SOM). In this study, two of these methods were used: HCA and PCA. They are explained below.

3.5.1 Hierarchical clustering analysis

HCA is a clustering method that uses a hierarchical dendrogram to display trends in the data. It is an agglomerative clustering technique where each feature is initialized to its own cluster and iteratively compared and “moved” near other clusters that are close in distance or highly correlated. Clusters are compared by a distance or correlation metric such as Euclidean distance or Pearson’s correlation with a linkage method. Common linkage methods include single linkage, complete linkage, and average linkage, where the minimum, maximum, or average of the distance or correlation metric between two clusters is used [21]. Agglomerative clustering also has no pre-defined number of clusters. After clustering has been performed, the dendrogram may be cut to create a specified number of clusters; however, this is not required. In this study, HCA was performed using the Pearson ($n - 1$) correlation metric with an average linkage method. Instead of a distance metric like Euclidean distance, the Pearson correlation metric was used to see similarity between metabolites and group metabolites based on correlations [22]. Furthermore, the average linkage method was chosen as it has been found to perform better than the single and complete linkage methods in gene set analysis [22]. HCA was performed on only significant to ANOVA metabolites in all organs; in addition, supervised sample wise HCA was performed to help identify outliers, where HCA was informed to cluster sample groups together.

3.5.2 Principal component analysis

PCA is a dimensionality reducing algorithm that helps identify sample group separation, sample outliers, metabolites contributing to group separation, and metabolite relationships. PCA utilizes singular value decomposition (SVD) or eigen decomposition of the correlation or covariance matrix to linearly transform the features into principal components (PCs) that represent the variance in the data. For a brief mathematical overview, PCA finds $n - 1$ (when $p \gg n$) principal components:

$$Z_j = X\phi_j \quad \text{where} \quad j = 1, \dots, n - 1 \quad (2)$$

where ϕ_j is the loading vector or the “weights” of each feature in the projected space and each principal component Z has decreasing variance - $Var(Z_1) \geq Var(Z_2) \geq \dots \geq Var(Z_{n-1})$ and is orthogonal to each other $PC\ Z_1 \perp Z_2 \perp \dots \perp Z_{n-1}$. This is very useful in metabolomics data analysis as there are typically hundreds to thousands of features being measured. Since the principal components represent the variability in the original dataset, they can be used as new features for analyses, instead of using all features. A certain number of PCs are chosen that cumulatively represent a high percentage of the variability in the data. PCA works best when between group variation is significantly more than within group variation - providing a means to discover groups and discover variables that separate these groups [23]. In the present study, metabolites solely significant to ANOVA were analyzed through PCA for each organ. SVD was utilized for the decomposition of the feature matrix and the first three principal components were analyzed and visualized. The scores (samples) plots were graphed to see group variation and look for sample outliers, and bi-plots were graphed to see metabolite correlations and to see contributions of metabolites to the group variation based off the cosine similarity metric.

3.6 Supervised methods

There are many supervised learning methods that can be implemented for metabolomics analyses such as support vector machines (SVM), partial least squares discriminant analysis (PLS-DA), orthogonal partial least squares discriminant analysis (OPLS-DA), and more [20]. The primary goal of these methods is to reduce dimensionality, build classifiers to predict class membership, find correlations between metabolites, and identify metabolites specifically contributing to group separation. The supervised method implemented in this study was PLS-DA.

3.6.1 Partial least squares discriminant analysis

To understand PLS-DA, it is important to understand PLS regression (PLS-R) as the only difference is that PLS-DA outputs discrete classes. PLS-R is widely used in a variety of chemometrics studies, where the number of features is far greater than the number of samples, and the features are highly correlated [24]. Thus, it is well suited for metabolomics. PLS-R is similar to the PCA model and aims to decompose two matrices, the feature matrix X and the response matrix y utilizing the same scores matrix T :

$$X = TP + E, \quad y = Tq + f \tag{3}$$

where E and f are residuals, and P and q are the loadings for the matrix X and vector y respectively. Following decomposition, each component of the model is calculated addi-

tively following the algorithm below [25]:

1. Calculate PLS weight vector:

$$w = X^T y$$

2. Calculate the scores:

$$t = \frac{Xw}{\sqrt{\sum w^2}}$$

3. Calculate the x loadings:

$$p = \frac{t^T X}{\sqrt{\sum t^2}}$$

4. Calculate the y loadings:

$$q = \frac{y^T t}{\sqrt{\sum t^2}}$$

5. Obtain X residual matrix:

$$X_{resid} = X - tp$$

6. Obtain y residual matrix:

$$y_{resid} = y - tq$$

7. Repeat for the max number of components specified with:

$$X = X_{resid} \quad \text{and} \quad y = y_{resid}$$

Then, using the regression relationship $y = X\beta + f = Tq + f$, it follows that \hat{y} can be predicted by:

$$\hat{y} = X\beta \tag{4}$$

where $\beta = W(PW)^{-1}q$. Overall, the PLS-DA method finds the metabolites (X variables) that best explain the maximum variation in the groups (y vector) and projects them into a reduced subspace. It is like PCA in that it produces both scores and loadings plots; however, PLS-DA tries to find the metabolites specifically causing the variance in the groups, whereas PCA is finding the maximum variance of all samples irrespective of the groups.

Because of the $p \gg n$ problem in metabolomics experiments, PLS-DA often results in a high number of misclassifications, and overfitting and validation procedures need to be

performed. In typical classification procedures, a dataset is broken up into a training set, testing set, and validation set. With small sample sizes, it is difficult to split the data into train, test, and validation splits. Many methods have been examined for best building PLS-DA models in metabolomics experiments [24, 26]. Two methods, a single cross validation (CV1) and double cross validation (CV2) [26, 27] have been found to perform best in selection of the number of dimensions (latent variables) and model quality assessment. In CV1, a traditional cross validation is performed where the samples are split into a training and validation set. Following, the training set is used to build multiple PLS-DA models with a maximum number of latent variables specified for the model parameters. The validation set is then tested on the models to select the optimal number of latent variables based off of some metric (i.e. number of misclassifications). When the best model has been selected, all samples are tested and the quality of the model is reported. However, this is not ideal as there is no unseen test set in this model and all samples are used in the training procedure. The other method, CV2, splits the data into a test set and a rest set. Then, the rest set is utilized in the traditional CV1 approach to identify the best number of latent variables. The best model is then tested on the held out test set. This is repeated such that every sample has been in the test set once, and a set of models are found. Often, this entire procedure is repeated and the best average quality across the k outer folds is selected. The CV2 approach is visualized in Figure 1 [27].

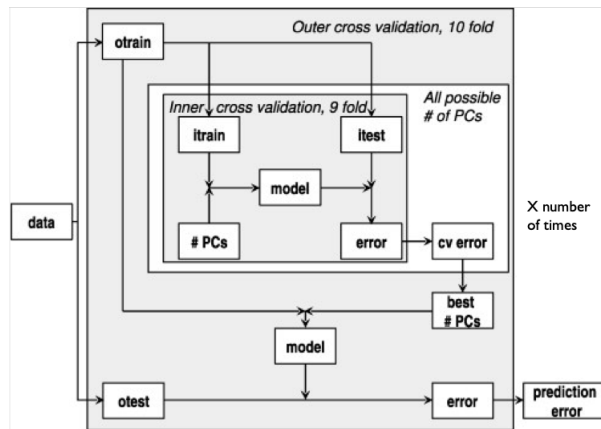


Figure 1: The double cross validation technique

Another problem with PLS-DA is that it is too "good" at separating data based on their classes. For example, given random data and random class assignment, PLS-DA can find a separation between these groups. Thus, separation of groups is meaningless, without further testing. To overcome this problem, permutation testing is done, where sample classes are randomly permuted (i.e. class are switched in the dataset, giving samples wrong

labels), PLS-DA is performed, and the error assessment metric is recorded. If such error metric for the non-permuted model is statistically significant compared to the permuted models, then a model can significant compared to models built on random data [24]. In the present study, PLS-DA was performed on each organ with CV2 validation where $k = 5$ on the inner CV loop and $k = 6$ on the outer CV loop. The number of misclassifications, NMC , error metric was used to evaluate the model:

$$NMC = FP + FN \quad (5)$$

where FP is the number of false positives (predicting AKI when there is not AKI) and FN is the number of false negatives (predicting sham or normal when there is AKI). Further, permutation testing was done 100 times to examine if the non-permuted data was statistically significant compared to the permuted data. The permutation p-values were calculated from:

$$P = \frac{1 + \#(NMC_p \leq NMC_{np})}{N} \quad (6)$$

where the NMC_p value is the NMC value for the permuted data, NMC_{np} is the NMC value for the non-permuted data, and N is the number of permutations.

3.7 Pathway enrichment analysis

After performing individual metabolite analysis, it is useful to generalize metabolites to their associated biochemical pathways since pathways are revealing of the relationships between individual metabolites and provide insight into the mechanisms being affected by an experimental condition. For example, the metabolite glucose is associated with a multitude of pathways, namely glycolysis, which includes a variety of metabolites related to the synthesis and decomposition of glucose. More than likely, multiple metabolites in glycolysis were measured in a metabolomics study, so pathways can be identified offering broader insight into the activity of the metabolome, irrespective of whether or not all metabolites in the pathway were measured. In pathway enrichment analysis, metabolites are associated with their meta-data from a biological database (i.e. the KEGG database). This meta-data includes the associated pathways of a particular metabolite. Then, enrichment analysis can take a list of metabolites with their concentration data to determine if a pathway is significantly active, under the assumption that this pathway is altered by the experimental conditions [28]. There are a few downsides to enrichment analysis, mainly that the algorithms are restricted to the pathway databases available and that there is no consensus on discriminating an up or down regulated pathway [29].

3.7.1 Pathway activity profiling

Pathway activity profiling (PAPi) is an enrichment analysis technique that calculates pathway activity scores (AS) for a given sample with a variety of metabolite concentration measurements. The algorithm finds the metabolites associated with every single pathway, and cross references those metabolites with the metabolites measured in the dataset [30]. Then, an activity score is calculated for each identified pathway in each sample:

$$S_A(P) = \frac{(r_1 + r_2 + \dots + r_n)N}{K} \quad (7)$$

where P is a pathway and r_1, \dots, r_n are the metabolites' concentrations measured in the pathway, N is the total number of metabolites identified via metabolomics and cross referenced with the pathway metabolites, and K is the total number of metabolites in the pathway. This score can be calculated for all samples under all experimental groups, and following, a t-test or ANOVA can be performed to see if there is statistical significance across sample groups' pathway activity scores. The PAPi algorithm has two assumptions - (i) the more metabolites identified by metabolomics means a higher path activity and (ii) the greater the activity of a pathway, the lower the concentration of the identified metabolites in the pathway. The second assumption is based off of higher pathway activity being characterized by metabolites in flux, since metabolites in flux would have higher conversion rates and thus lower abundances. This is not true for all pathways; specifically, glycolysis intermediates have been found to have high abundances in a high state of flux [30]. Because of the second assumption, activity scores are scaled to a reference condition and inverted. In the present study, PAPi was performed to identify pathways significantly altered in AKI in all organs utilizing the mouse pathway KEGG database and the normal group was used as the reference condition. ANOVA was performed to find pathways with significantly different activity scores across all groups. The activity scores were visualized in a heat map and hierarchical clustering was performed.

3.7.2 Metabolite set enrichment analysis

Metabolite Set Enrichment Analysis (MSEA) is another method to perform enrichment analysis on a metabolomic dataset. There are three well known methods for MSEA - over-representation analysis (ORA), quantitative enrichment analysis (QEA), and single sample profiling (SSP). ORA uses a list of significant metabolites to see if they are identifiable in metabolic pathways. QEA uses concentration data from multiple samples to determine significant pathways between two sample groups, and SSP is used for single samples and uses concentration data from a sample compared to normal concentration data to determine the significant pathways [31]. QEA was chosen for the present study. QEA selects path-

ways where a few metabolites are significantly changed or a lot of metabolites are slightly changed. Two methods exist for QEA, Goeman's global test and global ANCOVA. Both have been found to produce biologically meaningful results in gene set analysis and are relatively equal in power [32]. Goeman's global test was chosen for this study. It examines whether identified metabolites are predictive of a sample group (note that this only supports binary classification). Goeman's global test utilizes logistic regression [29]:

$$P(\hat{y}|\beta) = \sigma\left(\alpha + \sum_{j=1}^m x_{ij}\beta_j\right) \quad (8)$$

where β_j is the regression coefficient for the metabolite j , $j = 1, \dots, m$, and m is the number of metabolites identified in the pathway. To test whether there is a statistical effect on the experimental conditions is equivalent to testing $H_0 : \beta_1 = \beta_2 = \dots = \beta_m = 0$. However, this null hypothesis is not testable for $p \gg n$ problems, and Goeman overcomes this problem by the assumption that all coefficients belong to a common distribution resulting in testing that the covariance of this distribution is 0, $H_0 : \tau^2 = 0$ [33]. A Q statistic is utilized to determine the quality of the prediction. Permutation testing is done to examine if the Q statistic from the non-permuted results is significantly different from the permuted results. Lastly, an adjusted p-value is reported. In the present study, MSEA was performed using MetaboanalystR 2.0 [17], utilizing the mouse pathway database from KEGG and the Holm p-value adjustment. Pre-selected binary groups were compared, and the results were further explored to look for effect of AKI pathways by comparing the significant pathways identified in QEA, following Sig2AKI, IiAKI, OppInAKI, NoEfAKI criteria.

4 Results and Discussion

4.1 Time course of AKI

Serum creatinine and BUN were determined in normal mice and at each time point after sham and AKI. As shown in figure 2, serum creatinine was significantly increased at 4 and 24 hours post procedure in AKI versus sham and was not significantly different at 7 days; BUN was significantly increased in AKI versus sham at all three time points. Based off of these measurements, AKI was most prevalent at 24 hours.

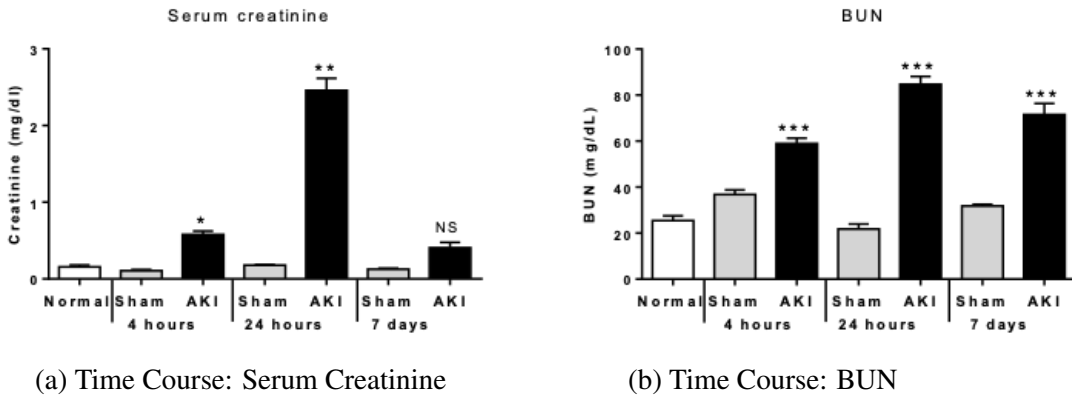


Figure 2: Time course of AKI. (A) Serum creatinine and (B) BUN were determined in normal controls and at 4 hour, 24 hours, and 7 days after Sham and AKI. (n=6 to 10). (One way ANOVA comparing the mean all groups with Tukey's multiple comparison test. Mean+/-SEM. * $P < 0.001$ vs. 4 hr Sham; ** $P < 0.0001$ vs. 24 hour sham; NS vs 7 day sham; *** $P < 0.0001$ vs. 4 hr Sham, 24 hour sham, or 7 day Sham respectively).

4.2 AKI and distant organ effects

4.2.1 Significant metabolites

Of the 343 of interest metabolites, 124, 141, 132, 177, and 128 were measured in the heart, lung, liver, kidney, and plasma, respectively.. Based on univariate ANOVA, 89, 95, 103, 142, and 119 were significantly different among experimental groups in the heart, lung, liver, kidney, and plasma respectively (see Table 1).

Organ	Number Metabolites Measured	Significant to ANOVA
Heart	124	89
Lung	141	95
Liver	132	103
Kidney	177	142
Plasma	128	119

Table 1: Metabolites significant to ANOVA by organ

Hierarchical clustering analysis (HCA) and principal component analysis (PCA) were performed for the significant to ANOVA metabolites for each organ to visualize overall trends in the data. The HCA heat maps for the heart, lung, liver, kidney, and plasma are shown in

supplementary section 6.1; the PCA scores plots and bi-plots are shown in supplementary section 6.2. Both HCA and PCA reveal that the most notable differences in metabolites occurred in the 24 hour AKI group for all organs with principal component (PC) 1 primarily explaining 24 hour AKI in the heart, PC 2 and PC 3 primarily explaining 24 hour AKI in the lung, PC 1 and PC 2 primarily explaining 24 hour AKI in the liver, PC 1 and PC 3 primarily explaining 24 hour AKI in the kidney, and PC 1 primarily explaining 24 hour AKI in the plasma. The metabolites with the highest sum of squared cosines between each principal component are listed in supplementary section 6.7

Additionally, PLS-DA was performed in order to identify the metabolites that are contributing to sample group separation (see section 6.8) and build a model to classify samples. PLS-DA was trained using the CV2 approach. The accuracies, NMC, precision, recall, component range, and permutation p-value results are reported for the five model sets built on the heart, lung, liver, kidney, and plasma in Table 2.

Organ	Accuracy	NMC	Precision	Recall	#Comp	P Value
Heart	93.84%	6.15%	88.89%	88.89%	6-15	$P < 0.01$
Lung	90.77%	9.23 %	85.71%	85.71%	10-16	$P < 0.01$
Liver	86.15%	13.85%	79.31%	76.67%	9-19	$P < 0.01$
Kidney	89.23%	10.77%	78.13%	78.13%	9-18	$P < 0.01$
Plasma	98.46%	1.54%	96.30%	96.30%	9-20	$P < 0.01$

Table 2: PLS-DA classification quality measures, model parameters, and permutation results

Overall, the best set of PLS-DA models to predict onset of AKI were the plasma classifiers.

4.2.2 Specific metabolites and metabolic pathways affected in distant organs by AKI

Specific metabolites affected by AKI (based off of the pre-defined effect of AKI groups: Sig2AKI, IiAKI, OppInAKI, NoEfAKI) in the heart, lung, liver, kidney, and plasma are shown in supplementary section 6.3. Overall, 53 (43%), 30 (21%), 43 (33%), 159 (90%), and 125 (98%) measured metabolites in the heart, lung, liver, kidney, and plasma respectively were affected by AKI. The most dramatic metabolic changes occurred at 24 hours for all organs, and are reported in table 3. At 4 hours, changes were not as severe in the heart, lung, and liver. Interestingly, metabolic effects were still noted 7 days post AKI, with larger changes in the kidney, plasma, and heart.

Furthermore, PAPi analysis was performed and activity scores for identified pathways were generated for every sample across all organs. HCA heat maps were created for

Organ	4 Hours I/D	24 Hours I/D	7 Days I/D
Heart	I:4 D:4	I:14 D:18	I:10 D:3
Lung	I:5 D:1	I:11 D:6	I:5 D:2
Liver	I:3 D:0	I:19 D:20	I:1 D:0
Kidney	I:26 D:35	I:25 D:34	I:22 D:17
Plasma	I:27 D:9	I:34 D:33	I:18 D:4

Table 3: Number of metabolites that were increased (I) or decreased (D) due to the effect of AKI

ANOVA significant pathways and are displayed in supplementary section 6.4 for the heart, lung, liver, kidney, and plasma. Additionally, MSEA QEA utilizing Goeman’s global test was performed and enriched pathways across all organs are displayed in supplementary section 6.5. There were a number of pathways enriched that were significant to AKI, as depicted in Table 4. The most dramatic pathway changes occurred at 24 hour AKI.

Organ	4 Hours	24 Hours	7 Days
Heart	3	25	1
Lung	0	1	0
Liver	0	10	15
Kidney	24	22	3
Plasma	11	30	0

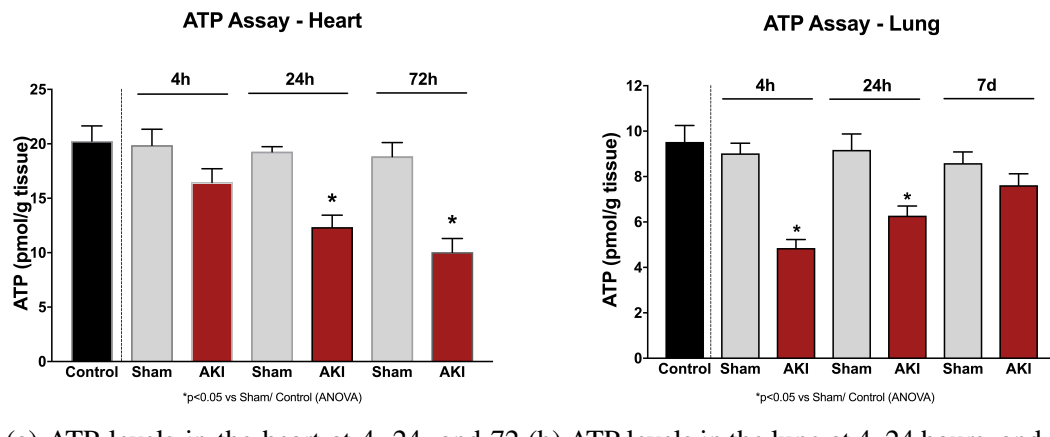
Table 4: Number of enriched pathways due to the effect of AKI

4.2.3 ATP levels in the heart and lung

ATP levels were measured in normal mice, sham, and AKI at 4, 24, and 72 hours (in a separate cohort of mice) in the heart and 4 and 24 hours, and 7 days in the lung. As shown in figure 3, ATP levels were significantly decreased at 24 hours after AKI in both the heart and lung. Additionally, ATP levels were still significantly decreased in the heart at 72 hours. Overall, ATP depletion foreshadows need to produce ATP via alternative energy metabolism.

4.2.4 Amino acid deficiencies

In the heart, several amino acids were decreased at 4 and 24 hours after AKI including alanine, aspartate, glutamate, glycine, and tyrosine, see box plots in supplementary sec-



(a) ATP levels in the heart at 4, 24, and 72 hours (b) ATP levels in the lung at 4, 24 hours, and 7 days

Figure 3: ATP levels in the heart and lung

tion 6.6.1. Additionally, several amino acid pathways were enriched including phenylalanine metabolism, lysine degradation, phenylalanine, tyrosine and tryptophan biosynthesis, glycine, serine and threonine metabolism, lysine biosynthesis, tyrosine metabolism, alanine, aspartate and glutamate metabolism, histidine metabolism, and more.

Amino acid depletion commonly occurs during cardiac ischemia and other forms of cardiac stress and reflects a number of injury-associated events such as ischemia reperfusion injury, ATP depletion, inadequate oxidative phosphorylation, increased alternative energy production, and increased oxidative stress [34, 35, 36]. In a normally functioning heart, amino acid metabolism contributes a very small percentage of ATP production; however, when oxidative phosphorylation is inadequate, as seen when there is decreased blood flow to the heart, amino acid metabolism increases and becomes an important source of ATP production [35]. In particular, glucogenic amino acids such as aspartate, glutamate, glycine, histidine, alanine, can be converted to glycolysis and TCA cycle intermediates to generate ATP. Other amino acids, histidine, trans-4-hydroxy-L-proline, and L-citrulline decreased in the sham group at 24 hours but no effect in AKI. Both L-citrulline and trans-4-hydroxy-L-proline are involved in arginine and proline metabolism, which ends in the production of glutamate. This pathway was intensified in AKI compared to sham suggesting the need to produce glutamate in AKI mediated heart injury.

The reduction in glutamate and aspartate is notable as these amino acids are reduced in cardiac biopsies in patients after cardiac bypass surgery and reductions are associated with ATP depletion and cardiac ischemia [34, 35, 36]. Additionally, the depletion of glycine is notable and has been seen to occur after myocardial infarction in rats [37]. Thus, decreased glutamate, aspartate, and glycine likely reflect ongoing amino acid metabolism, in addition

to the other decreases in glucogenic amino acids: alanine and tyrosine. Histidine, another glucogenic amino acid, only saw a decrease in the sham group. Many of these depletions, specifically of glutamate and glycine, is also suggestive of increased oxidative stress and an attempt to restore depleted glutathione stores (discussed further, below). There were a few amino acids depleted in the lung and liver. Of note, glutamate in the lung was decreased, which could also be suggestive of oxidative stress in the lung. Glutamate has a multitude of roles in metabolism, neurotransmission, and signaling, and its metabolism dysregulation has been observed in lung cancer patients [38, 39]. In the liver, serine was depleted, and two amino acid pathways were enriched: glycine, serine and threonine metabolism and arginine and proline metabolism. Serine depletion in the liver has been seen in patients with non-alcoholic fatty liver disease (NAFLD) [40]. See supplementary section 6.6.2 for box plots of glutamate and serine in the lung and liver.

4.2.5 Alternative energy metabolism

Metabolites involved in glycolysis, the citric acid (TCA) cycle, pentose phosphate pathway, and purine and pyrimidine metabolism were affected in the heart, lung, and liver after AKI and suggest a shift toward alternative energy production (non-oxidative energy production), in addition to the production of citric acid intermediates for use in oxidative phosphorylation. In the heart, increases in glucose, ribose, and pantothenate are indicative of the need to produce ATP, in addition to building the intermediates for the TCA cycle, which both produce ATP and are used downstream in oxidative phosphorylation. Further, intermediates in these pathways, such as 2-oxoglutarate and 3-oxalomalate saw significant increases in the heart. Malate, succinate, and D-glucose-6-phosphate also saw increases; however, did not meet the significance threshold. The pantothenate and CoA biosynthesis and pentose phosphate pathways were both enriched in the heart. In the lung, D-ribose and L-arabinose saw significant increases. The pentose and glucuronate interconversions pathway was also significantly enriched which interconnects arabinose to the pentose phosphate and citric acid cycle pathways. Interestingly, the liver showed opposite effects with glucose, glycolysis intermediates (D-glucose-6-phosphate, 3-oxalomalate, 2,3-bisphosphoglycerate, D-glyceraldehyde 3-phosphate), TCA cycle intermediates (malate), pentose phosphate pathway intermediates (5-phospho-alpha-D-ribose 1-diphosphate, 6-phospho-D-gluconate, D-glucono-1,5-lactone 6-phosphate) while maintaining increases in ribose, arabinose, pantothenate, and 2-hydroxyglutarate. The decrease in glucose in the liver is notable as this has been found to occur in fasting, where the liver will produce glucose via glycogenolysis [41]. Given the need for glucose in other organs to produce ATP, glycogenolysis in the liver is probable after AKI. See supplementary section 6.6.3 for box plots of alternative energy metabolites in all organs.

In the heart, energy shifts such as these are common during cardiac stress from multiple causes such as heart failure [42, 43], cardiac ATP depletion [44], myocardial ischemia/infarction, and myocarditis [45]. In the lung, this phenomenon is also seen in non-small cell lung cancer and in smokers basal cells [46]. In the liver, fasting [41], non-alcoholic steatohepatitis (NASH), and NAFLD [47] have been associated with alternative energy production as well.

Further, the increase in purine metabolism is seen by the decreases in purines adenine and adenosine in the heart (purines were not significantly decreased in the lung or liver) and accompanied by increases in their end products (5-hydroxyisourate and S-allantoin). All organs had increases in the purine degradation product S-allantoin. Further, pathway analysis found purine metabolism significantly enriched in the heart and liver. Pyrimidine consumption is also present as evidenced by increases in 5-6 dihydrothymine, an end product of pyrimidine metabolism, across all organs. Pyrimidine metabolism was enriched in the heart and liver as well. See supplementary section 6.6.4 for box plots of purine and pyrimidine metabolites in all organs.

4.2.6 Oxidative stress

In all organs, there were extensive indications of metabolite changes associated with oxidative stress after AKI, particularly at 24 hours. In the heart, increased oxidative stress is a common sign of cardiac stress and occurs in a wide range of diseases including myocardial infarction [37], myocarditis [45], dilated cardiomyopathy [48], and heart failure [49, 50]. In the lung, it has been related to asthma, inflammatory lung disease, COPD, acute lung injury, pulmonary fibrosis, and lung cancer [51, 52]. In the liver, oxidative stress has been found in chronic hepatitis C virus infection, alcoholic hepatitis, and NAFLD [53]. In both the heart and the liver, there was a significant decrease in glutathione (GSH). Though, not significant in the lung, an inhibitory effect of GSH seemed to occur at 24 hour AKI compared to the sham group. GSH is a potent anti-oxidant which is crucial to normal cardiac function [49, 50], lung function [52], and liver function [54]. Glutathione is a key defender against excess reactive oxygen species (ROS), which are detrimental to normal cellular function. Further, it is an early trigger of apoptotic cell death [55].

Additional markers of oxidative stress after AKI in the heart included increased 2-amino adipate (α -amino adipate), 5-hydroxyisourate, S-allantoin, ascorbate and decreased thioredoxin disulfide. In the lung, an increase in S-allantoin and decrease in thioredoxin disulfide was seen. In the liver, there was an increase in S-allantoin. α -amino adipate is a product of lysine degradation and a marker of protein oxidation [53, 56]. Its increase may be the result of oxidative stress and protein oxidation in addition to lysine degradation. The lysine degradation pathway was also found to be enriched in the heart. Purine

degradation leads to an increase in uric acid and downstream products 5-hydroxyisourate and S-allantoin via ROS-generating reactions [57]. Thus, increased S-allantoin is a strong biomarker for increased oxidative stress [58]. Ascorbate is significantly increased in the heart (the lung and liver saw non-significant increases), even though it itself is an anti-oxidant. This was also seen in rat models of heart failure [43]. See supplementary section 6.6.5 for box plots of oxidative stress metabolites in all organs.

4.3 Overall implications

Metabolomics analysis applied to AKI offers immense insight into the complex disease. This study demonstrates that AKI has substantial effects on the heart, lung, and liver, especially after 24 hours. In total, 43%, 21%, and 33% of metabolites measured were affected at some time point after AKI in the heart, lung, and liver respectively. Considering that only 124, 141, and 132 metabolites were identified from metabolomics analysis in the three organs in total, these percentages are substantial and outline drastic underlying changes post AKI, especially in the heart. Interestingly, the metabolites affected after AKI in the heart are similar to the changes seen after direct cardiac injury from myocardial ischemia reperfusion injury. This is corroborated by amino acid depletion, glutathione depletion, increased oxidative stress, and evidence of anaerobic energy production. Correspondingly, the lung also experienced similar effects, with amino acid, glutamate, being depleted significantly, glutathione depletion, increased oxidative stress, and markers of alternative energy production. In the liver, it was a similar story, with amino acid, serine, significantly depleted, glutathione depleted, increased oxidative stress, and signs of alternative energy metabolism. Overall, AKI causes energy substrate depletion, increased oxidative stress, and changes in energy metabolism in distant organs. Whether or not these changes are due to consumption or inhibited production of such substrates cannot be deduced from this study. However, given the lack of ATP in both the heart and the lung and the decrease of glucose in the liver, it is plausible that the substrates are being consumed for ATP generation.

Future studies should examine if supplementation of amino acids and/or antioxidants are a viable treatment option for AKI. In the heart, studies have been performed showing that during cardiac ischemia supplementation with glutamate and aspartate improves ATP production [36]. In the lung, amino acid supplementation has improved severe COPD and lung cancer outcomes [59, 60]. In terms of glutathione, it has been found to be essential for normal cardiac function [24, 50] and liver function [54], and supplementation is beneficial during hypoxia and bypass surgery [35]. In the lung, inhalation of glutathione has been found to address a number of lung diseases [61], though as indicated, further studies need to be performed. From a glucose perspective, its increase in both the heart and the lung

post AKI is indicative of increased glycolysis [30], and even though glucose is increased, its stores in the liver are depleted. Overall, the decreases in amino acids, antioxidants, and increases in glucose (decrease in the liver) are widespread after AKI, and mediations for such changes should be explored.

Currently, the supportive treatment of severe AKI, renal replacement therapy (RRT), which includes dialysis [62] is based around the random removal of metabolites from the blood, due to the fact that increases in metabolites are detrimental to distant organs and patient outcomes. Although the plasma did have 34 significantly increased metabolites, there were also 33 that were significantly decreased; thus, aimless removal of metabolites is not the only solution to treat AKI. Further, removal of already depleted metabolites such as amino acids, antioxidants, and glucose could harm the patient even more, as these metabolites are essential to normally functioning organs. Thus, a comprehensive, targeted approach to treatment of AKI that includes focused supplementation and removal should be explored as an alternative or in addition to RRT.

5 Concluding Remarks and Limitations

Overall, this study demonstrates that AKI is associated with dramatic changes in heart, lung, and liver metabolism, ATP depletion, and oxidative stress, with the most dramatic effects in the heart. While the complications of AKI are traditionally considered to be due to the accumulation of metabolites and treated via renal replacement therapy, this data demonstrate that numerous essential metabolites were not just increased but also depleted after AKI which likely contribute to the deleterious effects of AKI on distant organs. Methods to improve energy metabolism in these organs after AKI may have potential to improve outcomes and further studies should be performed. Furthermore, this data addresses and visualizes the complexity of AKI and suggest that more precise tools of mediation and treatment will be necessary to optimize patient outcomes. Finally, the plasma PLS-DA classifier model demonstrates the potential to assist diagnose AKI at time points as early as 4 hours.

Limitations: Metabolite levels reported reflect steady state levels that are the cumulative effect of numerous interconnected pathways. Definitive assessment of substrate sources for key metabolites and implications for metabolic pathways disrupted require additional focused experimentation. Accurate metabolite identity involves the use of appropriate standards, and may be subject to error. Raw data are available for review upon request.

References

- [1] D. S. Wishart, D. Tzur, C. Knox, R. Eisner, A. C. Guo, N. Young, D. Cheng, K. Jewell, D. Arndt, S. Sawhney, C. Fung, L. Nikolai, M. Lewis, M. A. Coutouly, I. Forsythe, P. Tang, S. Shrivastava, K. Jeroncic, P. Stothard, G. Amegbey, D. Block, D. D. Hau, J. Wagner, J. Miniaci, M. Clements, M. Gebremedhin, N. Guo, Y. Zhang, G. E. Duggan, G. D. Macinnis, A. M. Weljie, R. Dowlatabadi, F. Bamforth, D. Clive, R. Greiner, L. Li, T. Marrie, B. D. Sykes, H. J. Vogel, and L. Querengesser. Hmdb: the human metabolome database. *Nucleic Acids Res*, 35(Database issue):D521–6, 2007.
- [2] D. S. Wishart, Y. D. Feunang, A. Marcu, A. C. Guo, K. Liang, R. Vazquez-Fresno, T. Sajed, D. Johnson, C. Li, N. Karu, Z. Sayeeda, E. Lo, N. Assempour, M. Berjanskii, S. Singhal, D. Arndt, Y. Liang, H. Badran, J. Grant, A. Serra-Cayuela, Y. Liu, R. Mandal, V. Neveu, A. Pon, C. Knox, M. Wilson, C. Manach, and A. Scalbert. Hmdb 4.0: the human metabolome database for 2018. *Nucleic Acids Res*, 46(D1):D608–D617, 2018.
- [3] R. Murugan and J. A. Kellum. Acute kidney injury: what's the prognosis? *Nat Rev Nephrol*, 7(4):209–17, 2011.
- [4] Control Centers for Disease and Prevention. Hospitalization discharge diagnoses for kidney disease—united states, 1980–2005. *MMWR Morb Mortal Wkly Rep*, 57(12):309–12, 2008.
- [5] S. Nisula, K. M. Kaukonen, S. T. Vaara, A. M. Korhonen, M. Poukkunen, S. Karlsson, M. Haapio, O. Inkinen, I. Parviainen, R. Suojaranta-Ylinen, J. J. Laurila, J. Tenhunen, M. Reinikainen, T. Ala-Kokko, E. Ruokonen, A. Kuitunen, V. Pettila, and Finnaki Study Group. Incidence, risk factors and 90-day mortality of patients with acute kidney injury in finnish intensive care units: the finnaki study. *Intensive Care Med*, 39(3):420–8, 2013.
- [6] Va Nih Acute Renal Failure Trial Network, P. M. Palevsky, J. H. Zhang, T. Z. O’Connor, G. M. Chertow, S. T. Crowley, D. Choudhury, K. Finkel, J. A. Kellum, E. Paganini, R. M. Schein, M. W. Smith, K. M. Swanson, B. T. Thompson, A. Vijayan, S. Watnick, R. A. Star, and P. Peduzzi. Intensity of renal support in critically ill patients with acute kidney injury. *N Engl J Med*, 359(1):7–20, 2008.
- [7] Renal Replacement Therapy Study Investigators, R. Bellomo, A. Cass, L. Cole, S. Finfer, M. Gallagher, S. Lo, C. McArthur, S. McGuinness, J. Myburgh, R. Nor-

- ton, C. Scheinkestel, and S. Su. Intensity of continuous renal-replacement therapy in critically ill patients. *N Engl J Med*, 361(17):1627–38, 2009.
- [8] S. S. Waikar, K. D. Liu, and G. M. Chertow. Diagnosis, epidemiology and outcomes of acute kidney injury. *Clin J Am Soc Nephrol*, 3(3):844–61, 2008.
- [9] C. V. Thakar, A. Christianson, R. Freyberg, P. Almenoff, and M. L. Render. Incidence and outcomes of acute kidney injury in intensive care units: a veterans administration study. *Crit Care Med*, 37(9):2552–8, 2009.
- [10] T. S. Hoke, I. S. Douglas, C. L. Klein, Z. He, W. Fang, J. M. Thurman, Y. Tao, B. Dursun, N. F. Voelkel, C. L. Edelstein, and S. Faubel. Acute renal failure after bilateral nephrectomy is associated with cytokine-mediated pulmonary injury. *J Am Soc Nephrol*, 18(1):155–64, 2007.
- [11] M. E. Grams and H. Rabb. The distant organ effects of acute kidney injury. *Kidney Int*, 81(10):942–948, 2012.
- [12] R. Ologunde, H. Zhao, K. Lu, and D. Ma. Organ cross talk and remote organ damage following acute kidney injury. *Int Urol Nephrol*, 46(12):2337–45, 2014.
- [13] K. Lane, J. J. Dixon, I. A. MacPhee, and B. J. Philips. Renohepatic crosstalk: does acute kidney injury cause liver dysfunction? *Nephrol Dial Transplant*, 28(7):1634–47, 2013.
- [14] A. D’Alessandro, H. B. Moore, E. E. Moore, M. Wither, T. Nemkov, E. Gonzalez, A. Slaughter, M. Fragoso, K. C. Hansen, C. C. Silliman, and A. Banerjee. Early hemorrhage triggers metabolic responses that build up during prolonged shock. *Am J Physiol Regul Integr Comp Physiol*, 308(12):R1034–44, 2015.
- [15] Kieu Trinh Do, Simone Wahl, Johannes Raffler, Sophie Molnos, Michael Laimighofer, Jerzy Adamski, Karsten Suhre, Konstantin Strauch, Annette Peters, Christian Gieger, Claudia Langenberg, Isobel D Stewart, Fabian J Theis, Harald Grallert, Gabi Kastenmüller, and Jan Krumsiek. Characterization of missing values in untargeted ms-based metabolomics data and evaluation of missing data handling strategies. *Metabolomics*, 14(10):128, Sep 2018.
- [16] R. A. van den Berg, H. C. Hoefsloot, J. A. Westerhuis, A. K. Smilde, and M. J. van der Werf. Centering, scaling, and transformations: improving the biological information content of metabolomics data. *BMC Genomics*, 7:142, 2006.

- [17] J. Chong, M. Yamamoto, and J. Xia. Metaboanalystr 2.0: From raw spectra to biological insights. *Metabolites*, 9(3), 2019.
- [18] M. Vinaixa, S. Samino, I. Saez, J. Duran, J. J. Guinovart, and O. Yanes. A guideline to univariate statistical analysis for lc/ms-based untargeted metabolomics-derived data. *Metabolites*, 2(4):775–95, 2012.
- [19] Yoav Benjamini and Daniel Yekutieli. The control of the false discovery rate in multiple testing under dependency. *Ann. Statist.*, 29(4):1165–1188, 2001.
- [20] Sheng Ren, Anna A. Hinzman, Emily L. Kang, Rhonda D. Szczesniak, and Long Jason Lu. Computational and statistical analysis of metabolomics data. *Metabolomics*, 11(6):1492–1513, 2015.
- [21] Anil K Jain, M Narasimha Murty, and Patrick J Flynn. Data clustering: a review. *ACM computing surveys (CSUR)*, 31(3):264–323, 1999.
- [22] Pablo A. Jaskowiak, Ricardo JGB Campello, and Ivan G. Costa. On the selection of appropriate distances for gene expression data clustering. *BMC Bioinformatics*, 15(2):S2, 2014.
- [23] B. Worley and R. Powers. Multivariate analysis in metabolomics. *Curr Metabolomics*, 1(1):92–107, 2013.
- [24] Johan A. Westerhuis, Huub C. J. Hoefsloot, Suzanne Smit, Daniel J. Vis, Age K. Smilde, Ewoud J. J. van Velzen, John P. M. van Duijnhoven, and Ferdi A. van Dorsten. Assessment of plsda cross validation. *Metabolomics*, 4(1):81–89, Mar 2008.
- [25] Richard G Brereton and Gavin R Lloyd. Partial least squares discriminant analysis: taking the magic away. *Journal of Chemometrics*, 28(4):213–225, 2014.
- [26] Ewa Szymańska, Edoardo Saccenti, Age K Smilde, and Johan A Westerhuis. Double-check: validation of diagnostic statistics for pls-da models in metabolomics studies. *Metabolomics*, 8(Suppl 1):3–16, Jun 2012.
- [27] Suzanne Smit, Mariëlle J van Breemen, Huub C J Hoefsloot, Age K Smilde, Johannes M F G Aerts, and Chris G de Koster. Assessing the statistical validity of proteomics based biomarkers. *Anal Chim Acta*, 592(2):210–7, Jun 2007.
- [28] Sean C Booth, Aalim M Weljie, and Raymond J Turner. Computational tools for the secondary analysis of metabolomics experiments. *Comput Struct Biotechnol J*, 4:e201301003, 2013.

- [29] Jelle J. Goeman, Sara A. van de Geer, Floor de Kort, and Hans C. van Houwelingen. A global test for groups of genes: testing association with a clinical outcome. *Bioinformatics*, 20(1):93–99, 01 2004.
- [30] Raphael B M Aggio, Katya Ruggiero, and Silas Granato Villas-Bôas. Pathway activity profiling (papi): from the metabolite profile to the metabolic pathway activity. *Bioinformatics*, 26(23):2969–76, Dec 2010.
- [31] Arnald Alonso, Sara Marsal, and Antonio Julià. Analytical methods in untargeted metabolomics: state of the art in 2015. *Front Bioeng Biotechnol*, 3:23, 2015.
- [32] U Mansmann and R Meister. Testing differential gene expression in functional groups. goeman’s global test versus an ancova approach. *Methods Inf Med*, 44(3):449–53, 2005.
- [33] Antonio Rosato, Leonardo Tenori, Marta Cascante, Pedro Ramon De Atauri Carulla, Vitor A P Martins Dos Santos, and Edoardo Saccetti. From correlation to causation: analysis of metabolomics data using systems biology approaches. *Metabolomics*, 14(4):37, 2018.
- [34] M S Suleiman, W C Dihmis, M Caputo, G D Angelini, and A J Bryan. Changes in myocardial concentration of glutamate and aspartate during coronary artery surgery. *Am J Physiol*, 272(3 Pt 2):H1063–9, Mar 1997.
- [35] Kenneth J Drake, Veniamin Y Sidorov, Owen P McGuinness, David H Wasserman, and John P Wikswo. Amino acids as metabolic substrates during cardiac ischemia. *Exp Biol Med (Maywood)*, 237(12):1369–78, Dec 2012.
- [36] A Venturini, R Ascione, H Lin, E Polesel, G D Angelini, and M-S Suleiman. The importance of myocardial amino acids during ischemia and reperfusion in dilated left ventricle of patients with degenerative mitral valve disease. *Mol Cell Biochem*, 330(1-2):63–70, Oct 2009.
- [37] Xingxing Wang, Dian Wang, Jiayan Wu, Xiaojun Yu, Junyao Lv, Jing Kong, Guanghui Zhu, and Ruibing Su. Metabolic characterization of myocardial infarction using gc-ms-based tissue metabolomics. *Int Heart J*, 58(3):441–446, May 2017.
- [38] Yeon-Kyung Choi and Keun-Gyu Park. Targeting glutamine metabolism for cancer treatment. *Biomol Ther (Seoul)*, 26(1):19–28, Jan 2018.

- [39] Slawomir Michalak, Joanna Rybacka-Mossakowska, Wojciech Ambrosius, Joanna Gazdulska, Iwona Gołda-Gocka, Wojciech Kozubski, and Rodryg Ramlau. The markers of glutamate metabolism in peripheral blood mononuclear cells and neurological complications in lung cancer patients. *Dis Markers*, 2016:2895972, 2016.
- [40] Adil Mardinoglu, Rasmus Agren, Caroline Kampf, Anna Asplund, Mathias Uhlen, and Jens Nielsen. Genome-scale metabolic modelling of hepatocytes reveals serine deficiency in patients with non-alcoholic fatty liver disease. *Nat Commun*, 5:3083, 2014.
- [41] Liangyou Rui. Energy metabolism in the liver. *Compr Physiol*, 4(1):177–97, Jan 2014.
- [42] Torsten Doenst, Tien Dung Nguyen, and E Dale Abel. Cardiac metabolism in heart failure: implications beyond atp production. *Circ Res*, 113(6):709–24, Aug 2013.
- [43] Brian E Sansbury, Angelica M DeMartino, Zhengzhi Xie, Alan C Brooks, Robert E Brainard, Lewis J Watson, Andrew P DeFilippis, Timothy D Cummins, Matthew A Harbeson, Kenneth R Brittan, Sumanth D Prabhu, Aruni Bhatnagar, Steven P Jones, and Bradford G Hill. Metabolomic analysis of pressure-overloaded and infarcted mouse hearts. *Circ Heart Fail*, 7(4):634–42, Jul 2014.
- [44] Joanne S Ingwall and Robert G Weiss. Is the failing heart energy starved? on using chemical energy to support cardiac function. *Circ Res*, 95(2):135–45, Jul 2004.
- [45] Núria Gironès, Sofía Carbajosa, Néstor A Guerrero, Cristina Poveda, Carlos Chillón-Marinas, and Manuel Fresno. Global metabolomic profiling of acute myocarditis caused by trypanosoma cruzi infection. *PLoS Negl Trop Dis*, 8(11):e3337, Nov 2014.
- [46] Suzanne M Cloonan and Augustine M K Choi. Mitochondria in lung disease. *J Clin Invest*, 126(3):809–20, Mar 2016.
- [47] Zoe Schofield, Michelle Ac Reed, Philip N Newsome, David H Adams, Ulrich L Günther, and Patricia F Lalor. Changes in human hepatic metabolism in steatosis and cirrhosis. *World J Gastroenterol*, 23(15):2685–2695, Apr 2017.
- [48] Keiko Maekawa, Akiyoshi Hirayama, Yuko Iwata, Yoko Tajima, Tomoko Nishimaki-Mogami, Shoko Sugawara, Noriko Ueno, Hiroshi Abe, Masaki Ishikawa, Mayumi Murayama, Yumiko Matsuzawa, Hiroki Nakanishi, Kazutaka Ikeda, Makoto Arita, Ryo Taguchi, Naoto Minamino, Shigeo Wakabayashi, Tomoyoshi Soga, and Yoshiro Saito. Global metabolomic analysis of heart tissue in a hamster model for dilated cardiomyopathy. *J Mol Cell Cardiol*, 59:76–85, Jun 2013.

- [49] Christophe Adamy, Paul Mulder, Lara Khouzami, Nathalie Andrieu-abadie, Nicole Defer, Gabriele Candiani, Catherine Pavoine, Philippe Caramelle, Richard Souk-tani, Philippe Le Corvoisier, Magali Perier, Matthias Kirsch, Thibaud Damy, Alain Berdeaux, Thierry Levade, Christian Thuillez, Luc Hittinger, and Françoise Pecker. Neutral sphingomyelinase inhibition participates to the benefits of n-acetylcysteine treatment in post-myocardial infarction failing heart rats. *J Mol Cell Cardiol*, 43(3):344–53, Sep 2007.
- [50] Thibaud Damy, Matthias Kirsch, Lara Khouzami, Philippe Caramelle, Philippe Le Corvoisier, Françoise Roudot-Thoraval, Jean-Luc Dubois-Randé, Luc Hittinger, Catherine Pavoine, and Françoise Pecker. Glutathione deficiency in cardiac patients is related to the functional status and structural cardiac abnormalities. *PLoS One*, 4(3):e4871, 2009.
- [51] Hee Sun Park, So Ri Kim, and Yong Chul Lee. Impact of oxidative stress on lung diseases. *Respirology*, 14(1):27–38, Jan 2009.
- [52] I Rahman and W MacNee. Oxidative stress and regulation of glutathione in lung inflammation. *Eur Respir J*, 16(3):534–54, Sep 2000.
- [53] Sha Li, Hor-Yue Tan, Ning Wang, Zhang-Jin Zhang, Lixing Lao, Chi-Woon Wong, and Yibin Feng. The role of oxidative stress and antioxidants in liver diseases. *Int J Mol Sci*, 16(11):26087–124, Nov 2015.
- [54] Yasushi Honda, Takaomi Kessoku, Yoshio Sumida, Takashi Kobayashi, Takayuki Kato, Yuji Ogawa, Wataru Tomono, Kento Imajo, Koji Fujita, Masato Yoneda, Koshi Kataoka, Masataka Taguri, Takeharu Yamanaka, Yuya Seko, Saiyu Tanaka, Satoru Saito, Masafumi Ono, Satoshi Oeda, Yuichiro Eguchi, Wataru Aoi, Kenji Sato, Yoshito Itoh, and Atsushi Nakajima. Efficacy of glutathione for the treatment of nonalcoholic fatty liver disease: an open-label, single-arm, multicenter, pilot study. *BMC Gastroenterol*, 17(1):96, Aug 2017.
- [55] R Franco and J A Cidlowski. Apoptosis and glutathione: beyond an antioxidant. *Cell Death Differ*, 16(10):1303–14, Oct 2009.
- [56] Isabella Dalle-Donne, Daniela Giustarini, Roberto Colombo, Ranieri Rossi, and Aldo Milzani. Protein carbonylation in human diseases. *Trends Mol Med*, 9(4):169–76, Apr 2003.
- [57] Kwangsoo Kim, Jinseo Park, and Sangkee Rhee. Structural and functional basis for (s)-allantoin formation in the ureide pathway. *J Biol Chem*, 282(32):23457–64, Aug 2007.

- [58] H Kaur and B Halliwell. Action of biologically-relevant oxidizing species upon uric acid. identification of uric acid oxidation products. *Chem Biol Interact*, 73(2-3):235–47, 1990.
- [59] R W Dal Negro, A Testa, R Aquilani, S Tognella, E Pasini, A Barbieri, and F Boschi. Essential amino acid supplementation in patients with severe copd: a step towards home rehabilitation. *Monaldi Arch Chest Dis*, 77(2):67–75, Jun 2012.
- [60] M P K J Engelen, A M Safar, T Bartter, F Koeman, and N E P Deutz. High anabolic potential of essential amino acid mixtures in advanced nonsmall cell lung cancer. *Ann Oncol*, 26(9):1960–6, Sep 2015.
- [61] Jonathan Prouskey. The treatment of pulmonary diseases and respiratory-related conditions with inhaled (nebulized or aerosolized) glutathione. *Evid Based Complement Alternat Med*, 5(1):27–35, Mar 2008.
- [62] Sarah Faubel, Lakhmir S Chawla, Glenn M Chertow, Stuart L Goldstein, Bertrand L Jaber, Kathleen D Liu, and Acute Kidney Injury Advisory Group of the American Society of Nephrology. Ongoing clinical trials in aki. *Clin J Am Soc Nephrol*, 7(5):861–73, May 2012.

6 Supplementary Material

6.1 HCA

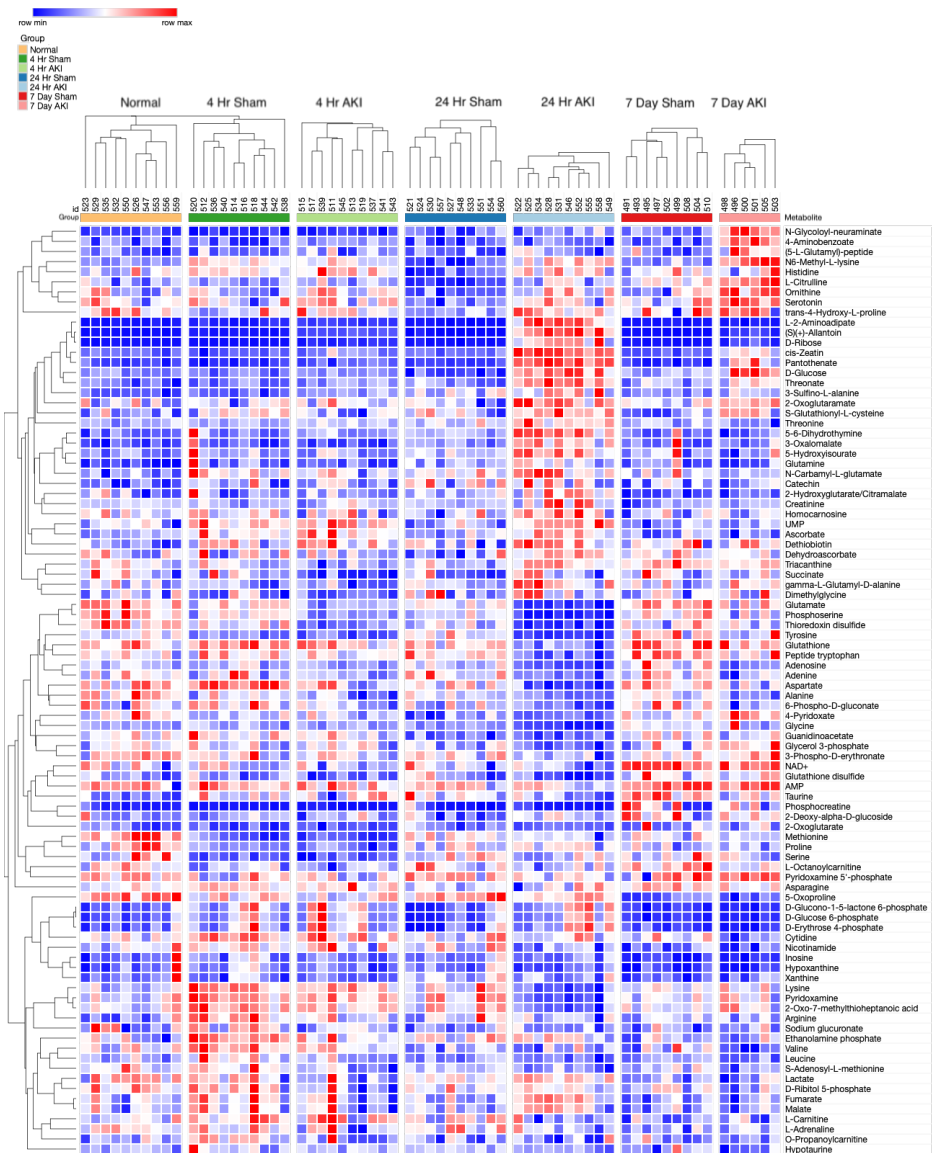


Figure 4: Heart HCA of ANOVA significant metabolites (Pearson ($n-1$) correlation metric with average linkage), red is row maximum (metabolite concentration), white is row medium, blue is row minimum

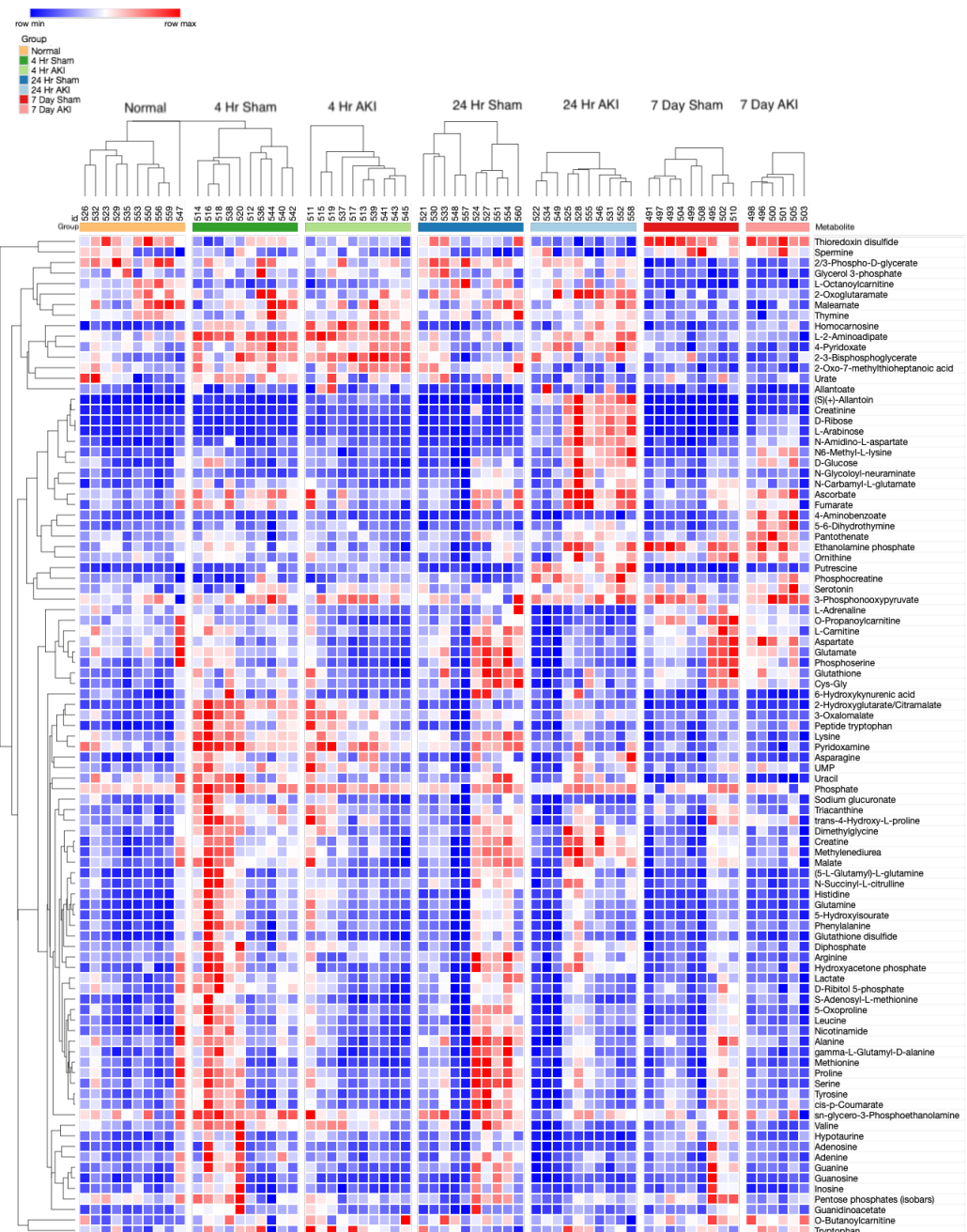


Figure 5: Lung HCA of ANOVA significant metabolites (Pearson (n-1) correlation metric with average linkage), red is row maximum (metabolite concentration), white is row medium, blue is row minimum

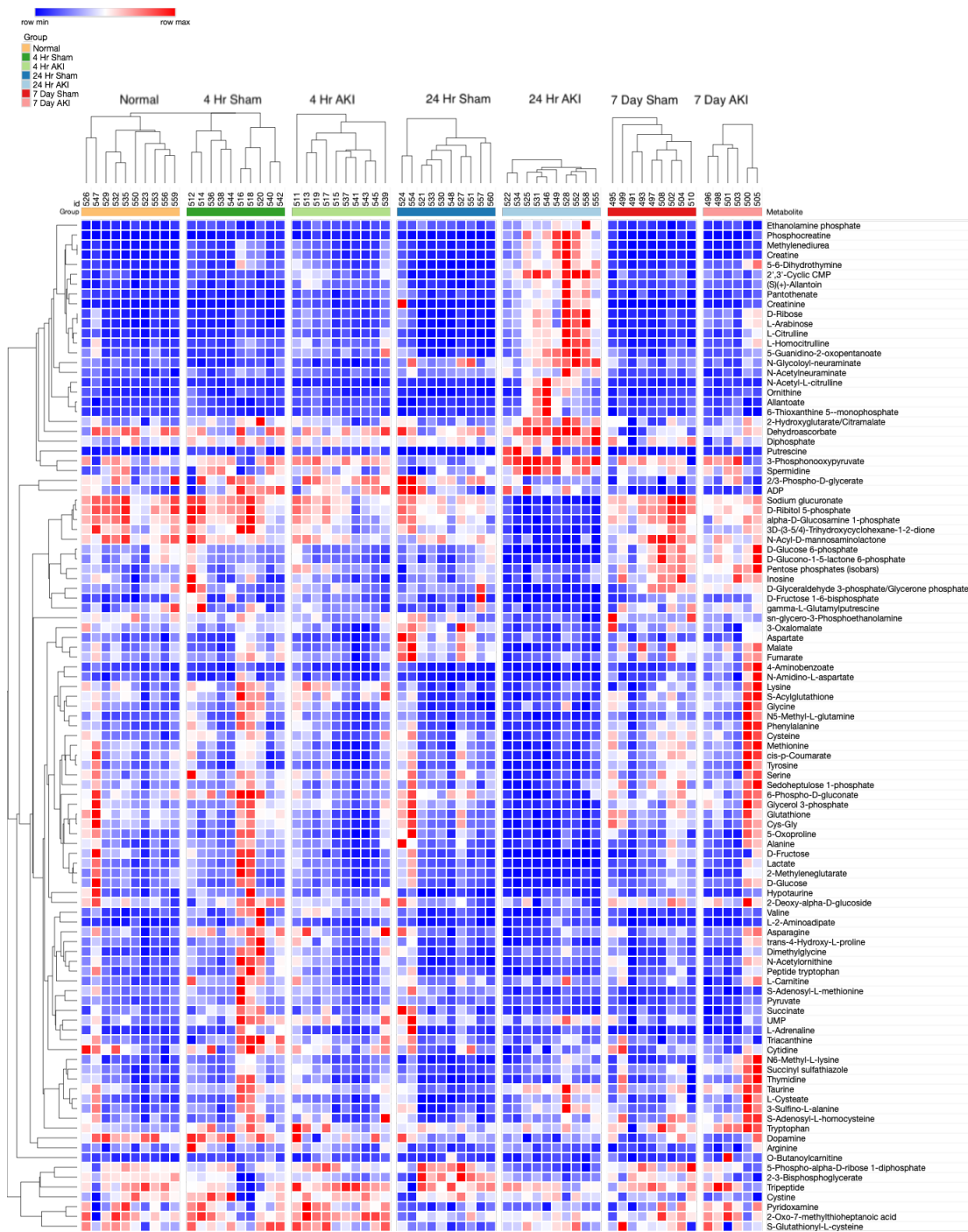


Figure 6: Liver HCA of ANOVA significant metabolites (Pearson (n-1) correlation metric with average linkage), red is row maximum (metabolite concentration), white is row medium, blue is row minimum

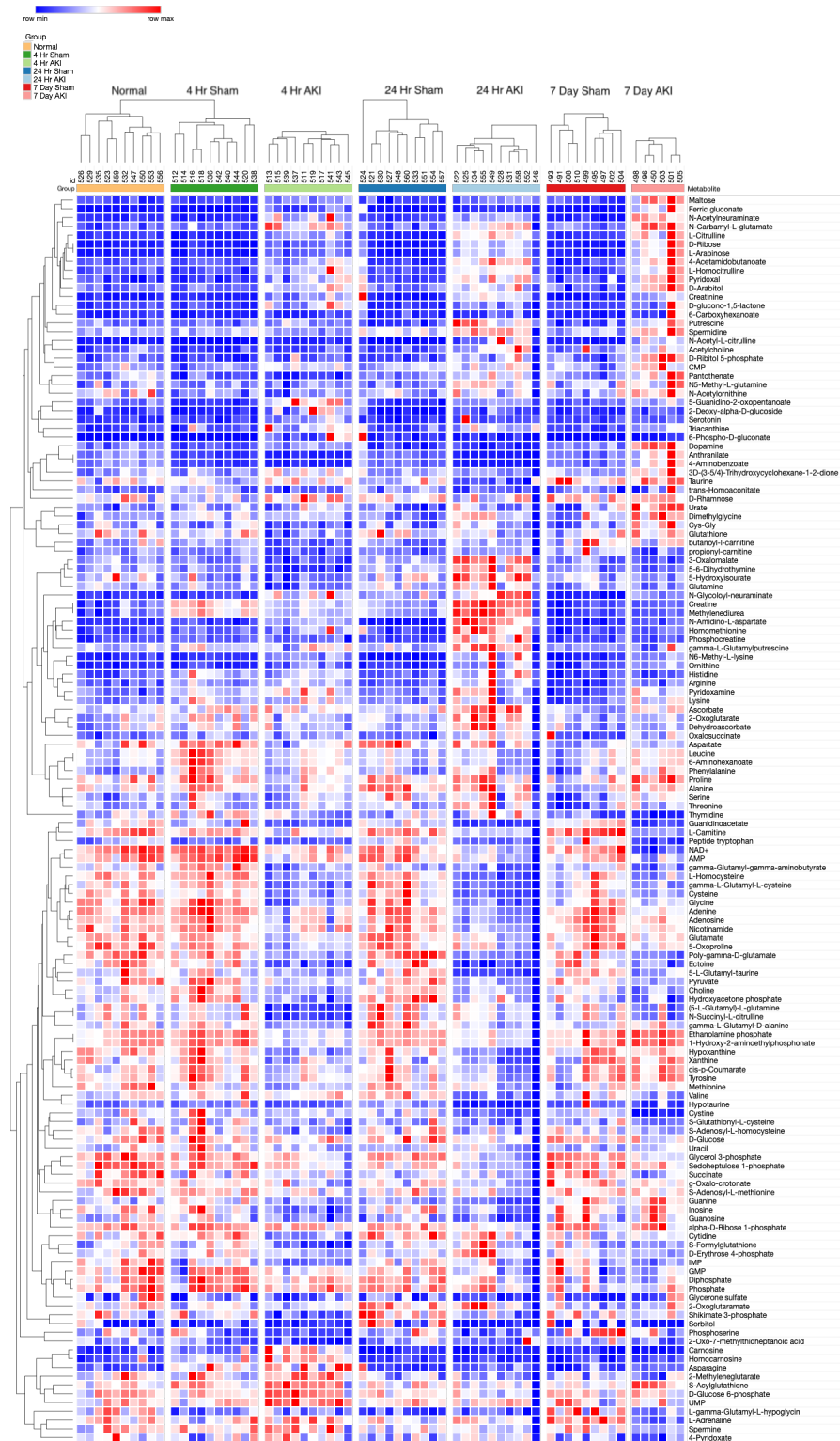


Figure 7: Kidney HCA of ANOVA significant metabolites (Pearson ($n-1$) correlation metric with average linkage), red is row maximum (metabolite concentration), white is row medium, blue is row minimum

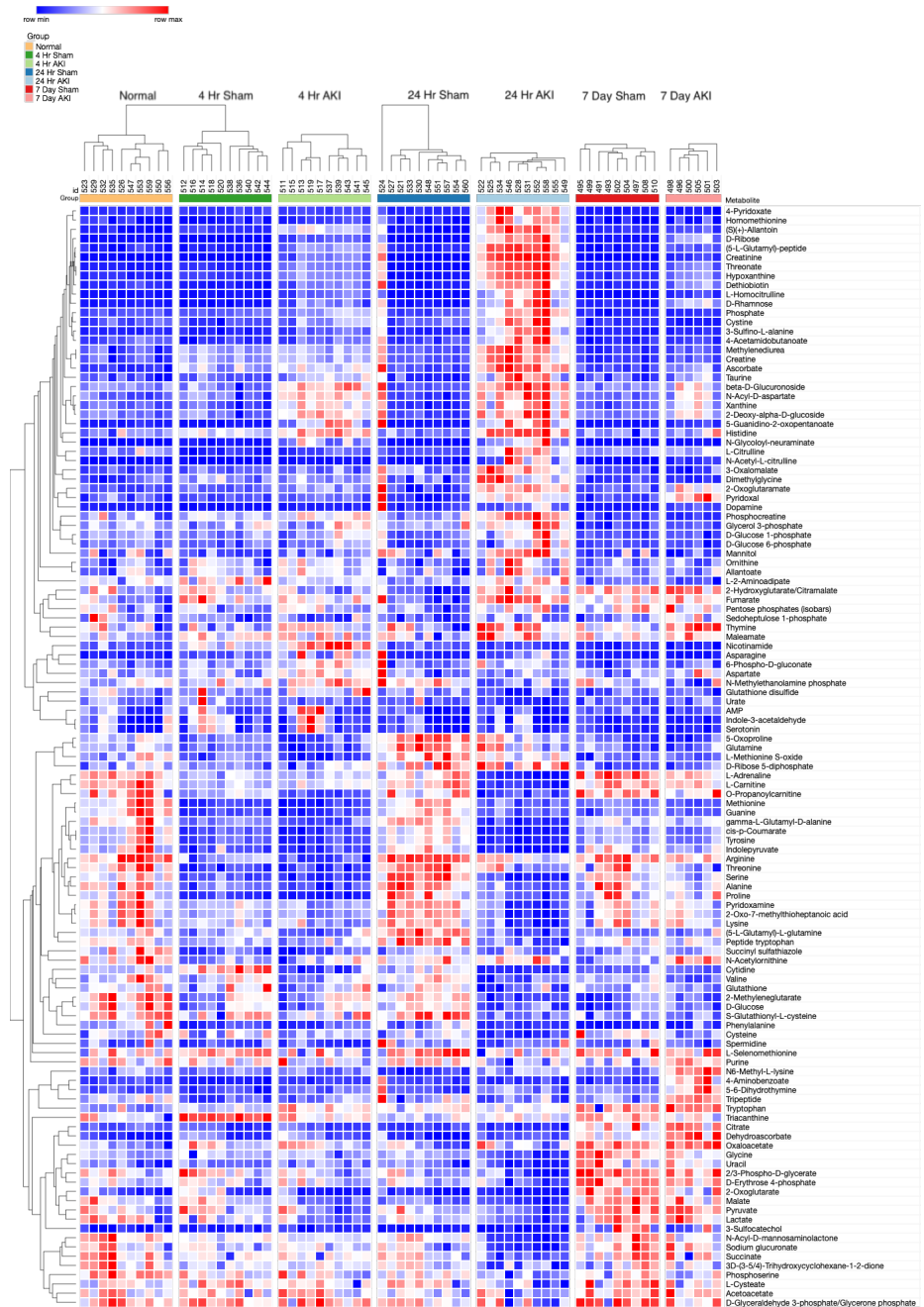


Figure 8: Plasma HCA of ANOVA significant metabolites (Pearson (n-1) correlation metric with average linkage), red is row maximum (metabolite concentration), white is row medium, blue is row minimum

6.2 PCA

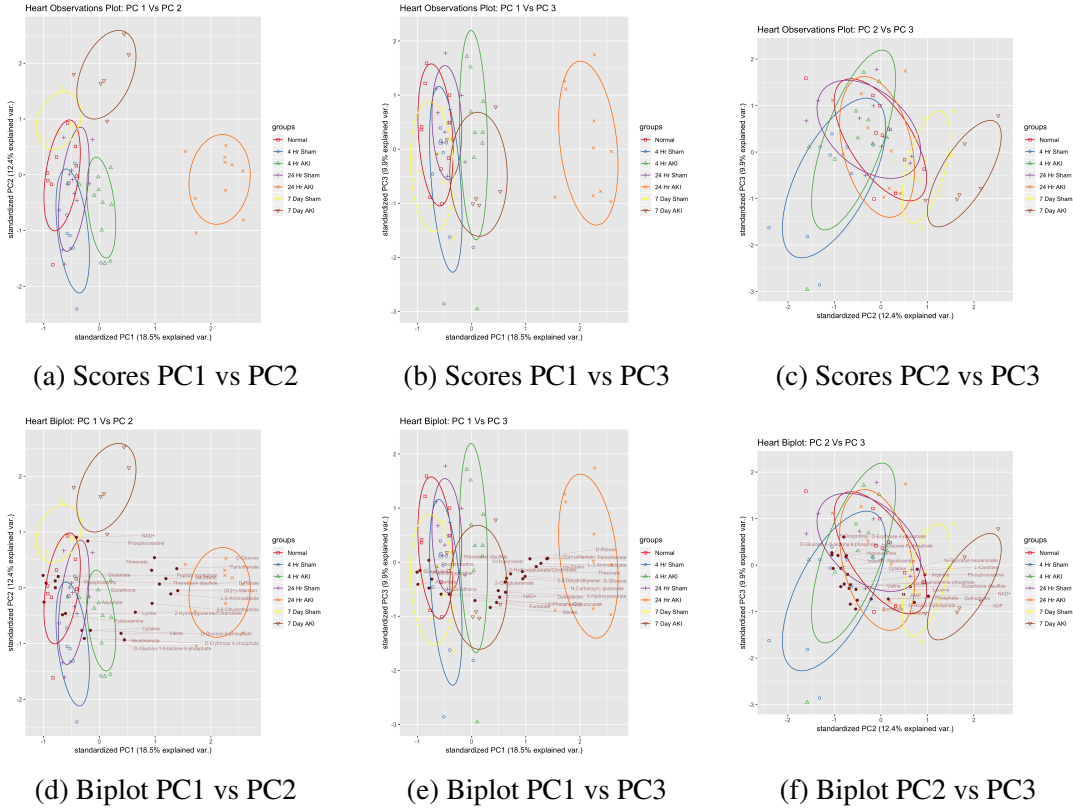


Figure 9: Heart PCA Scores and Biplots, PCA utilizing SVD, the first three components were graphed and respectively account for 18.5%, 12.4%, and 9.9% of the variance in the data. Biplots show the top 25 metabolites with the highest sum of squared cosine values between the two components graphed

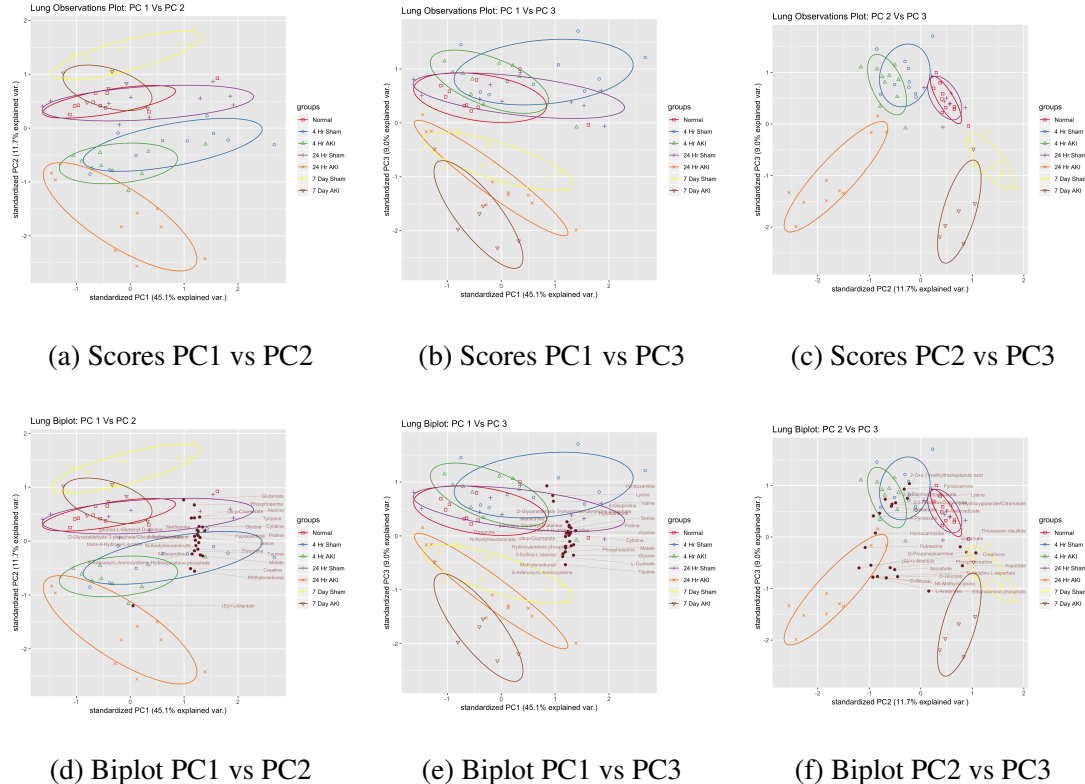


Figure 10: Lung PCA Scores and Biplots, PCA utilizing SVD, the first three components were graphed and respectively account for 45.1%, 11.7%, and 9.0% of the variance in the data. Biplots show the top 25 metabolites with the highest sum of squared cosine values between the two components graphed

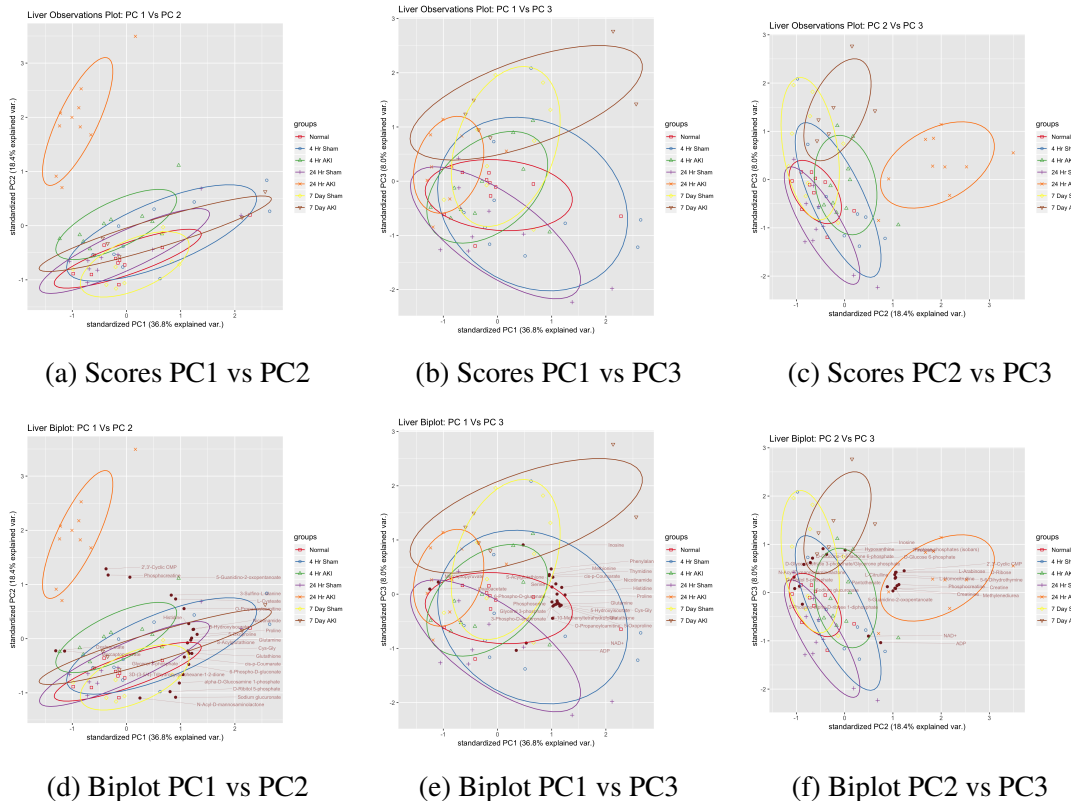
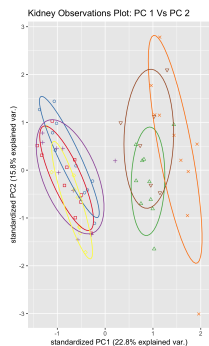
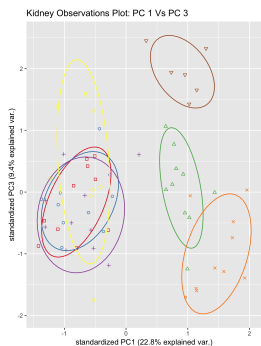


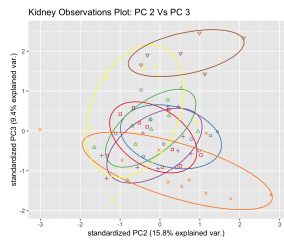
Figure 11: Liver PCA Scores and Biplots, PCA utilizing SVD, the first three components were graphed and respectively account for 36.8%, 18.4%, and 8.0% of the variance in the data. Biplots show the top 25 metabolites with the highest sum of squared cosine values between the two components graphed



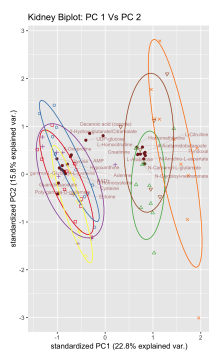
(a) Scores PC1 vs PC2



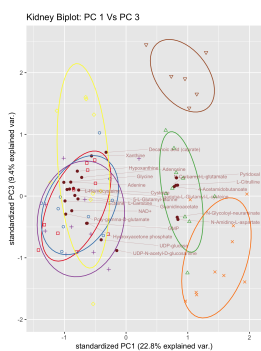
(b) Scores PC1 vs PC3



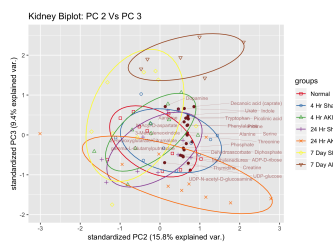
(c) Scores PC2 vs PC3



(d) Biplot PC1 vs PC2



(e) Biplot PC1 vs PC3



(f) Biplot PC2 vs PC3

Figure 12: Kidney PCA Scores and Biplots, PCA utilizing SVD, the first three components were graphed and respectively account for 22.8%, 15.8%, and 9.4% of the variance in the data. Biplots show the top 25 metabolites with the highest sum of squared cosine values between the two components graphed

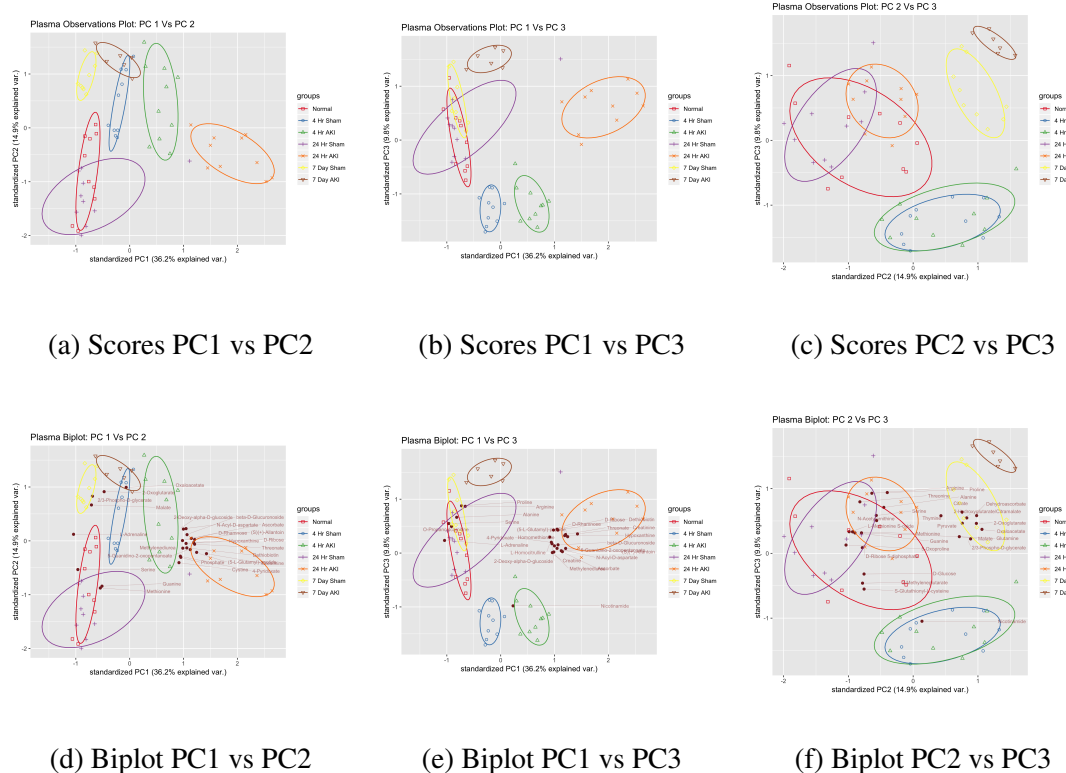


Figure 13: Plasma PCA Scores and Biplots, PCA utilizing SVD, the first three components were graphed and respectively account for 36.2%, 14.9%, and 9.8% of the variance in the data. Biplots show the top 25 metabolites with the highest sum of squared cosine values between the two components graphed

6.3 Effect of AKI metabolites

4 Hours			
	Heart	Lung	Liver
Increased	D-Ribose ¹ 3-Sulfino-L-alanine ¹ L-2-Amino adipate ¹ (S)(+)-Allantoin ²	D-Ribose ¹ L-Arabinose ¹ Creatinine ¹ (S)(+)-Allantoin ² Homocarnosine ²	(S)(+)-Allantoin ¹ 2',3'-Cyclic CMP ¹ Creatinine ¹
Decreased	Glutamate ¹ Succinate ¹ Phosphoserine ¹ Thioredoxin disulfide ¹	2-Hydroxyglutarate/Citramalate ³	

Table 5: Metabolites that were increased or decreased due to the effect of AKI at 4 hours in the heart, lung, or liver, 1: Sig2AKI, 2: LiAKI, 3: OppInAKI, 4: NoEfAKI

24 Hours

	Heart	Lung	Liver
Increased	(S)(+)-Allantoin ¹ UMP ¹ D-Ribose ¹ 2-Oxoglutaramate ¹ Ascorbate ¹ Pantothenate ¹ cis-Zeatin ¹ L-2-Aminoadipate ¹ Threonate ¹ 5-Hydroxyisourate ² 5-6-Dihydrothymine ² 3-Oxalomalate ² D-Glucose ³ N6-Methyl-L-lysine ³	(S)(+)-Allantoin ¹ 5-6-Dihydrothymine ¹ 4-Pyridoxate ¹ D-Ribose ¹ Putrescine ¹ L-Arabinose ¹ Homocarnosine ¹ Phosphocreatine ¹ Creatinine ¹ N6-Methyl-L-lysine ¹ N-Amidino-L-aspartate ¹	(S)(+)-Allantoin ¹ 2',3'-Cyclic CMP ¹ 5-6-Dihydrothymine ¹ D-Ribose ¹ 2-Hydroxyglutarate/Citramalate ¹ 3-Phosphonooxypyruvate ¹ L-Citrulline ¹ Putrescine ¹ Spermidine ¹ L-Arabinose ¹ 5-Guanidino-2-oxopentanoate ¹ Phosphocreatine ¹ Creatine ¹ Creatinine ¹ N-Acetyl-L-citrulline ¹ Pantothenate ¹ Methylenediurea ¹ L-Homocitrulline ¹ Ethanolamine phosphate ²
Decreased	Aspartate ¹ Glycine ¹ Lysine ¹ Tyrosine ¹ Adenine ¹ Adenosine ¹ Glutathione ¹ Peptide tryptophan ¹ Pyridoxamine ¹ 2-Oxo-7-methylthioheptanoic acid ¹ Alanine ² Glutamate ² Phosphoserine ² Thioredoxin disulfide ² Histidine ⁴ L-Citrulline ⁴ trans-4-Hydroxy-L-proline ⁴ Serotonin ⁴	Glutamate ¹ Hypotaurine ¹ L-Carnitine ¹ O-Propanoylcarnitine ¹ Thioredoxin disulfide ¹ 2-Oxo-7-methylthioheptanoic acid ¹	Serine ¹ D-Glucose 6-phosphate ¹ D-Glyceraldehyde 3-phosphate/Glycerone phosphate ¹ 2-3-Bisphosphoglycerate ¹ Malate ¹ 6-Phospho-D-gluconate ¹ D-Glucono-1,5-lactone 6-phosphate ¹ 5-Phospho-alpha-D-ribose 1-diphosphate ¹ Glutathione ¹ S-Adenosyl-L-methionine ¹ alpha-D-Glucosamine 1-phosphate ¹ 3D-(3-5/4)-Trihydroxycyclohexane-1,2-dione ¹ Glycerol 3-phosphate ¹ sn-glycero-3-Phosphoethanolamine ¹ 2-Methyleneglutarate ¹ 3-Oxalomalate ¹ cis-p-Coumarate ¹ N-Acyl-D-mannosaminolactone ¹ Sodium glucuronate ¹ D-Ribitol 5-phosphate ¹

Table 6: Metabolites that were increased or decreased due to the effect of AKI at 24 hours in the heart, lung, or liver, 1: Sig2AKI, 2: IiAKI, 3: OppInAKI, 4: NoEfAKI

7 Days			
	Heart	Lung	Liver
Increased	(S)(+)-Allantoin ¹ D-Glucose ¹ 2-Oxoglutaramate ¹ Ornithine ¹ L-Citrulline ¹ N-Glycoloyl-neuraminate ¹ Serotonin ¹ cis-Zeatin ¹ 4-Aminobenzoate ¹ N6-Methyl-L-lysine ¹	(S)(+)-Allantoin ¹ Phosphocreatine ¹ N6-Methyl-L-lysine ¹ N-Amidino-L-aspartate ¹ Hypotaurine ⁴	Putrescine ¹
Decreased	Alanine ¹ Cytidine ¹ Adenosine ¹	D-Ribose ⁴ L-Arabinose ⁴	

Table 7: Metabolites that were increased or decreased due to the effect of AKI at 7 days in the heart, lung, or liver, 1: Sig2AKI, 2: IiAKI, 3: OppInAKI, 4: NoEfAKI

Kidney			
	4 Hour	24 Hour	7 Day
Increase			
UMP ¹	Histidine ¹	Urate ¹	
Pyridoxal ¹	Pyridoxal ¹	Pyridoxal ¹	
Maltose ¹	Maltose ¹	Maltose ¹	
D-Ribose ¹	D-Ribose ¹	D-Ribose ¹	
D-Arabitol ¹	Ornithine ¹	D-Arabitol ¹	
Ornithine ¹	L-Citrulline ¹	Ornithine ¹	
N-Acetylneuraminate ¹	N-Acetylneuraminate ¹	L-Citrulline ¹	
N-Glycoloyl-neuraminate ¹	L-Arabinose ¹	Putrescine ¹	
L-Arabinose ¹	Phosphocreatine ¹	N-Acetylneuraminate ¹	
Homocarnosine ¹	Creatine ¹	L-Arabinose ¹	
Carnosine ¹	4-Acetamidobutanoate ¹	Creatinine ¹	
Creatinine ¹	N-Acetyl-L-citrulline ¹	4-Acetamidobutanoate ¹	
4-Acetamidobutanoate ¹	Triacanthine ¹	N-Acetyl-L-citrulline ¹	
Serotonin ¹	3-Oxalomalate ¹	Dopamine ¹	
Triacanthine ¹	Oxalosuccinate ¹	Triacanthine ¹	
N6-Methyl-L-lysine ¹	N-Carbamyl-L-glutamate ¹	N6-Methyl-L-lysine ¹	
D-glucono-1,5-lactone ¹	L-Homocitrulline ¹	Ferric gluconate ¹	
Ferric gluconate ¹	Homomethionine ¹	D-Ribitol 5-phosphate ¹	
N-Amidino-L-aspartate ¹	N-Glycoloyl-neuraminate ²	Pyridoxamine ¹	
N-Carbamyl-L-glutamate ¹	Methylenediuera ²	N-Carbamyl-L-glutamate ¹	
L-Homocitrulline ¹	Putrescine ³	L-Homocitrulline ¹	
L-Citrulline ³	N6-Methyl-L-lysine ³	N-Glycoloyl-neuraminate ³	
5-Guanidino-2-oxopentanoate ³	N-Amidino-L-aspartate ³		
N-Acetyl-L-citrulline ³	Choline ⁴		
Leucine ⁴	Hydroxyacetone phosphate ⁴		
6-Aminohexanoate ⁴			

Table 8: Metabolites that were increased due to the effect of AKI at all time points in the kidney 1: Sig2AKI, 2: IiAKI, 3: OppInAKI, 4: NoEfAKI

Kidney			
	4 Hour	24 Hour	7 Day
Decrease	Cysteine ¹ Glutamate ¹ Glycine ¹ Adenine ¹ Cytidine ¹ Inosine ¹ Hypoxanthine ¹ 5-6-Dihydrothymine ¹ NAD+ ¹ Sedoheptulose 1-phosphate ¹ Glutathione ¹ 5-Oxoproline ¹ gamma-L-Glutamyl-L-cysteine ¹ gamma-L-Glutamyl-D-alanine ¹ (5-L-Glutamyl)-L-glutamine ¹ L-Homocysteine ¹ N-Succinyl-L-citrulline ¹ Guanidinoacetate ¹ Ectoine ¹ Ethanolamine phosphate ¹ Choline ¹ L-Carnitine ¹ 1-Hydroxy-2-aminoethylphosphonate ¹ 3-Oxalomalate ¹ S-Formylglutathione ¹ Shikimate 3-phosphate ¹ Poly-gamma-D-glutamate ¹ Hydroxyacetone phosphate ¹ IMP ² Anthranilate ² 4-Aminobenzoate ² gamma-Glutamyl-gamma-aminobutyrate ³ Creatine ³ Methylenediurea ³ Dopamine ⁴	Cysteine ¹ Glutamate ¹ Glycine ¹ Valine ¹ Cystine ¹ AMP ¹ Adenosine ¹ Adenine ¹ GMP ¹ Guanine ¹ Inosine ¹ Hypoxanthine ¹ Nicotinamide ¹ NAD+ ¹ Pyruvate ¹ alpha-D-Ribose 1-phosphate ¹ gamma-L-Glutamyl-L-cysteine ¹ 5-L-Glutamyl-taurine ¹ L-Homocysteine ¹ Guanidinoacetate ¹ Taurine ¹ Hypotaurine ¹ Anthranilate ¹ g-Oxalo-crotonate ¹ Ectoine ¹ Glycerol 3-phosphate ¹ Ethanolamine phosphate ¹ L-Carnitine ¹ 1-Hydroxy-2-aminoethylphosphonate ¹ 4-Aminobenzoate ¹ Peptide tryptophan ¹ cis-p-Coumarate ¹ Poly-gamma-D-glutamate ¹ Sedoheptulose 1-phosphate ²	Cystine ¹ Adenine ¹ Thymidine ¹ IMP ¹ NAD+ ¹ Pyruvate ¹ Succinate ¹ gamma-Glutamyl-gamma-aminobutyrate ¹ L-gamma-Glutamyl-L-hypoglycin ¹ Spermine ¹ Guanidinoacetate ¹ L-Adrenaline ¹ Ectoine ¹ Glycerol 3-phosphate ¹ L-Carnitine ¹ Peptide tryptophan ¹ Poly-gamma-D-glutamate ¹

Table 9: Metabolites that were decreased due to the effect of AKI at all time points in the kidney 1: Sig2AKI, 2: IiAKI, 3: OppInAKI, 4: NoEfAKI

Plasma	4 Hour	24 Hour	7 Day
Increase			
	Aspartate ¹	Histidine ¹	Hypoxanthine ¹
	Histidine ¹	Cystine ¹	Thymine ¹
	Tryptophan ¹	Hypoxanthine ¹	Pyridoxal ¹
	Cystine ¹	Xanthine ¹	D-Ribose ¹
	Xanthine ¹	(S)(+)-Allantoin ¹	D-Rhamnose ¹
	Phosphate ¹	Pyridoxal ¹	2-Oxoglutaramate ¹
	2-Oxoglutaramate ¹	4-Pyridoxate ¹	(5-L-Glutamyl)-peptide ¹
	6-Phospho-D-gluconate ¹	Phosphate ¹	Creatinine ¹
	(5-L-Glutamyl)-peptide ¹	D-Ribose ¹	N-Acetyl-L-citrulline ¹
	5-Guanidino-2-oxopentanoate ¹	D-Rhamnose ¹	Dopamine ¹
	Creatinine ¹	2-Oxoglutaramate ¹	4-Aminobenzoate ¹
	Taurine ¹	Fumarate ¹	2-Deoxy-alpha-D-glucoside ¹
	3-Sulfino-L-alanine ¹	Ascorbate ¹	N6-Methyl-L-lysine ¹
	2-Deoxy-alpha-D-glucoside ¹	(5-L-Glutamyl)-peptide ¹	Dethiobiotin ¹
	N-Acyl-D-aspartate ¹	Dimethylglycine ¹	Threonate ¹
	beta-D-Glucuronoside ¹	L-Citrulline ¹	5-6-Dihydrothymine ²
	L-Homocitrulline ¹	N-Glycoloyl-neuraminate ¹	Tripeptide ³
	Hypoxanthine ²	5-Guanidino-2-oxopentanoate ¹	L-Homocitrulline ³
	(S)(+)-Allantoin ²	Phosphocreatine ¹	
	Nicotinamide ²	Creatine ¹	
	N-Glycoloyl-neuraminate ²	Creatinine ¹	
	Threonate ²	4-Acetamidobutanate ¹	
	D-Ribose ³	N-Acetyl-L-citrulline ¹	
	D-Rhamnose ³	Taurine ¹	
	Dethiobiotin ³	3-Sulfino-L-alanine ¹	
	Tripeptide ³	Methylenediurea ¹	
	Triacanthine ⁴	3-Oxalomalate ¹	
		Dethiobiotin ¹	
		Threonate ¹	
		N-Acyl-D-aspartate ¹	
		beta-D-Glucuronoside ¹	
		L-Homocitrulline ¹	
		Homomethionine ¹	
		5-Oxoproline ⁴	

Table 10: Metabolites that were increased due to the effect of AKI at all time points in the plasma 1: Sig2AKI, 2: IiAKI, 3: OppInAKI, 4: NoEfAKI

Plasma	4 Hour	24 Hour	7 Day
Decrease			
	Malate ¹	Alanine ¹	Valine ¹
	L-Methionine S-oxide ¹	Arginine ¹	Methionine ²
	O-Propanoylcarnitine ¹	Cysteine ¹	5-Guanidino-2-oxopentanoate ⁴
	Arginine ²	Glycine ¹	N-Acetylornithine ⁴
	Cytidine ³	Lysine ¹	
	L-Citrulline ⁴	Methionine ¹	
	4-Acetamidobutanoate ⁴	Phenylalanine ¹	
	Dopamine ⁴	Proline ¹	
	4-Aminobenzoate ⁴	Tyrosine ¹	
		Valine ¹	
		Guanine ¹	
		Cytidine ¹	
		D-Glucose ¹	
		Lactate ¹	
		Succinate ¹	
		S-Glutathionyl-L-cysteine ¹	
		gamma-L-Glutamyl-D-alanine ¹	
		Indolepyruvate ¹	
		L-Adrenaline ¹	
		L-Carnitine ¹	
		O-Propanoylcarnitine ¹	
		2-Methyleneglutarate ¹	
		cis-p-Coumarate ¹	
		N-Acyl-D-mannosaminolactone ¹	
		Sodium glucuronate ¹	
		Pyridoxamine ¹	
		2-Oxo-7-methylthioheptanoic acid ¹	
		Malate ²	
		Phosphoserine ²	
		Serine ³	
		(5-L-Glutamyl)-L-glutamine ³	
		Peptide tryptophan ³	
		N6-Methyl-L-lysine ⁴	

Table 11: Metabolites that were decreased due to the effect of AKI at all time points in the plasma 1: Sig2AKI, 2: IiAKI, 3: OppInAKI, 4: NoEfAKI

6.4 PAPi HCA

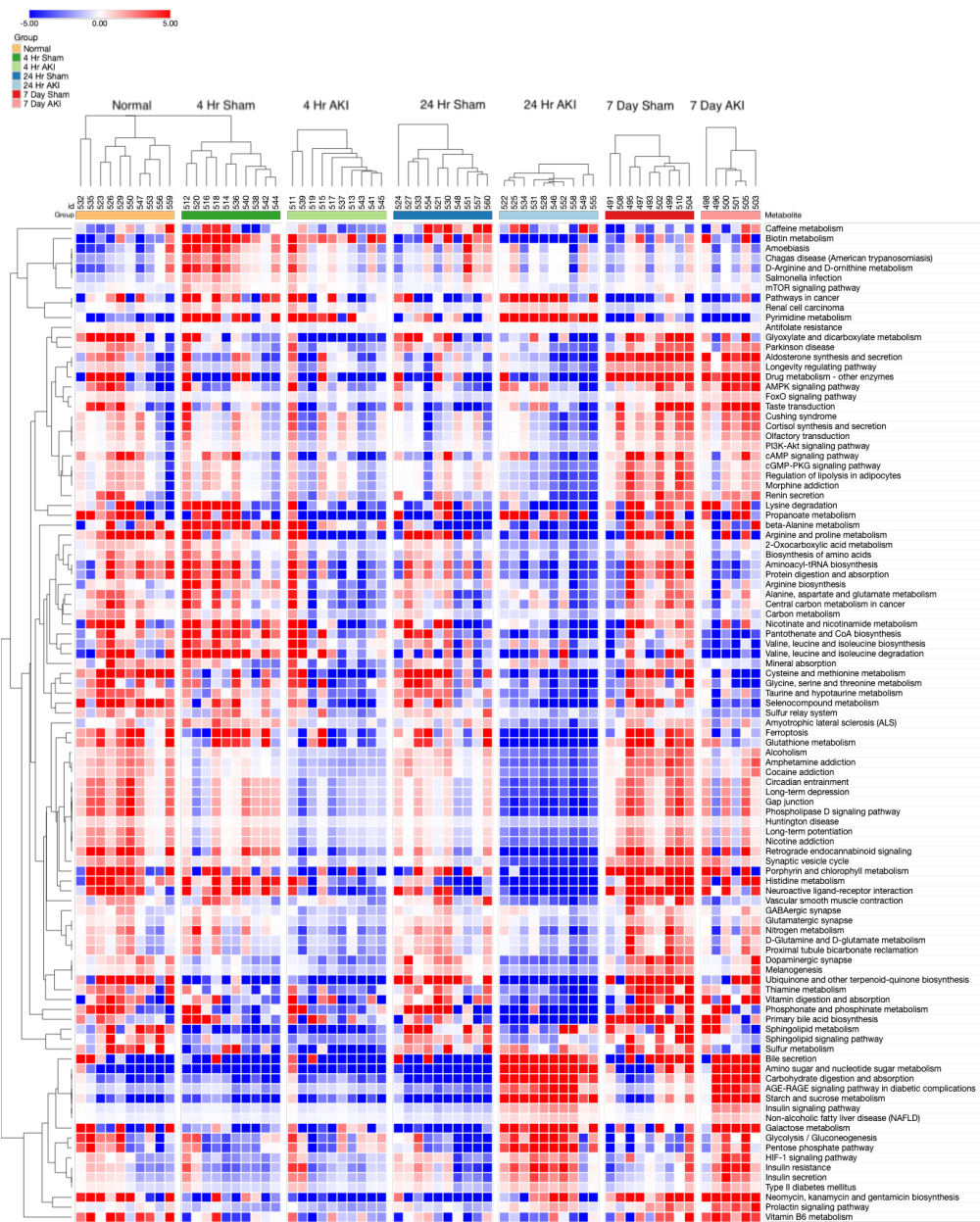


Figure 14: Heart HCA of PAPi (pearson ($n-1$) correlation metric with average linkage), red is activity score ($AS > 0$ (not enriched), white is $AS = 0$, blue is $AS < 0$ (enriched))

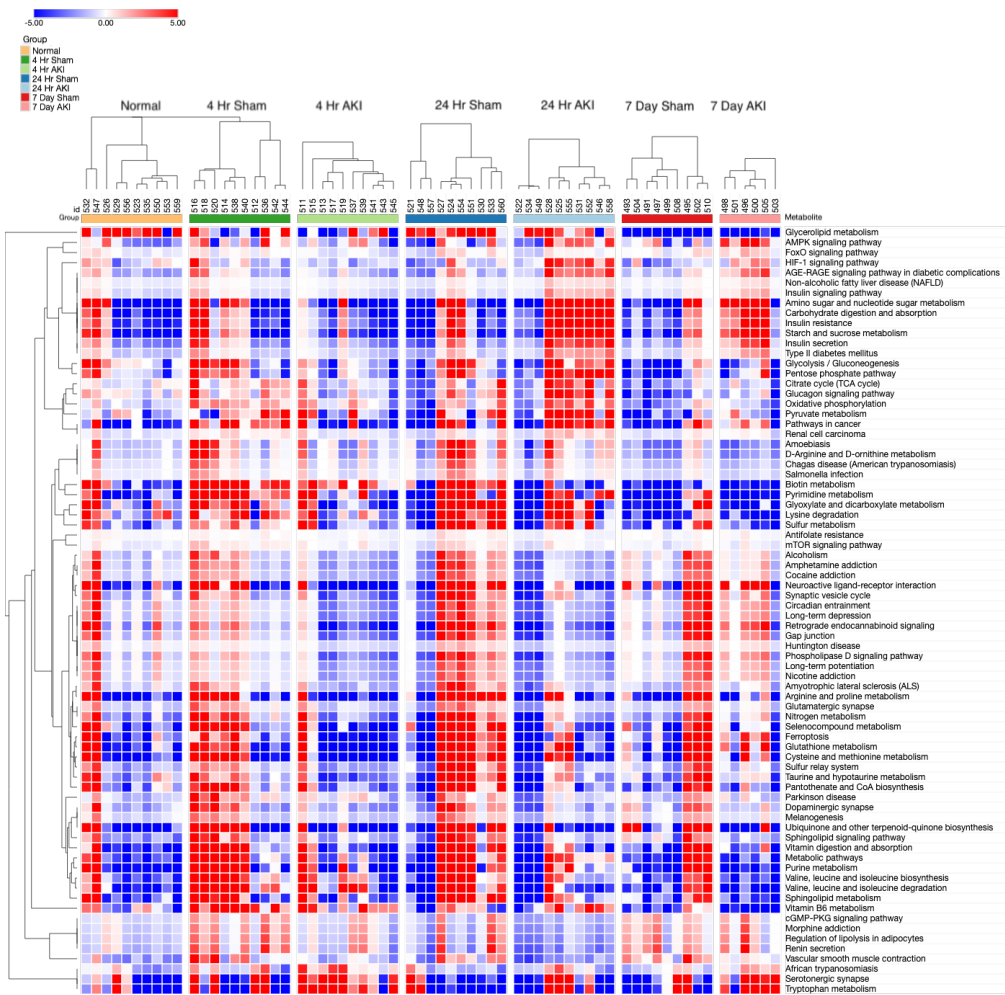


Figure 15: Lung HCA of PAPi (pearson (n-1) correlation metric with average linkage), red is activity score (AS) > 0 (not enriched), white is AS = 0, blue is AS < 0 (enriched)

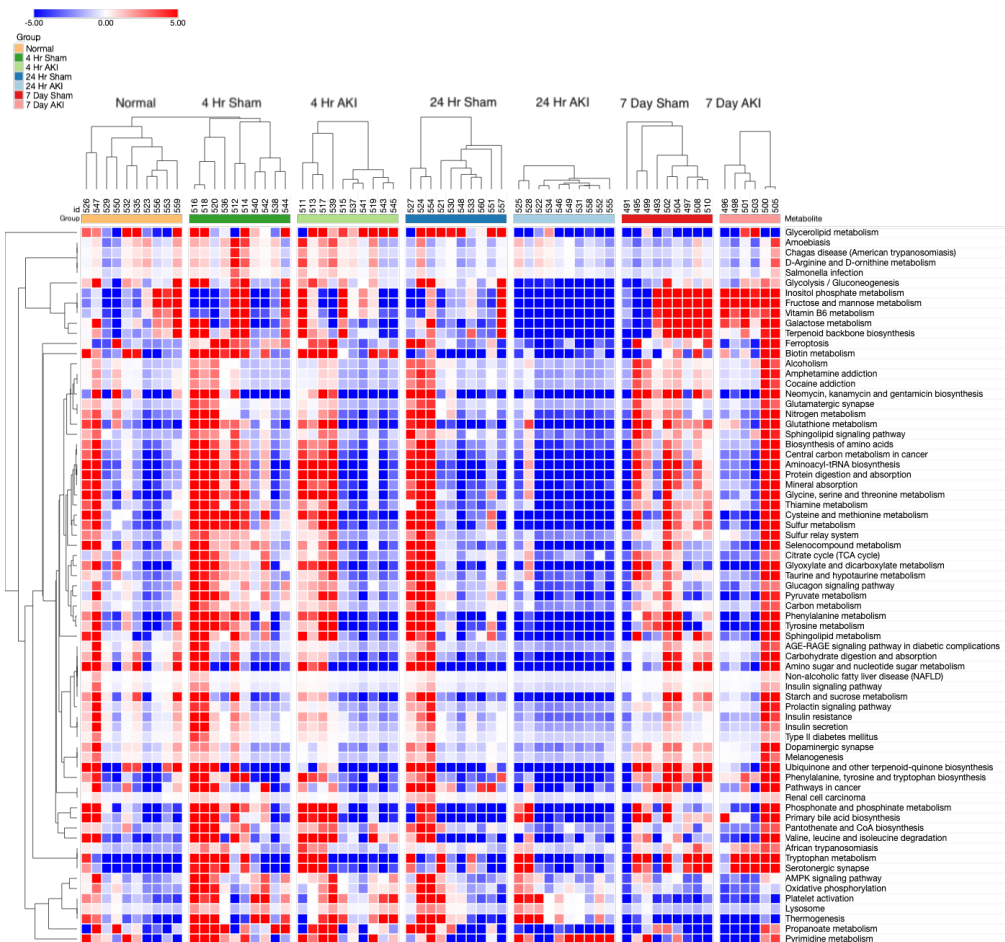


Figure 16: Liver HCA of PAPi (pearson ($n-1$) correlation metric with average linkage), red is activity score ($AS > 0$ (not enriched), white is $AS = 0$, blue is $AS < 0$ (enriched))

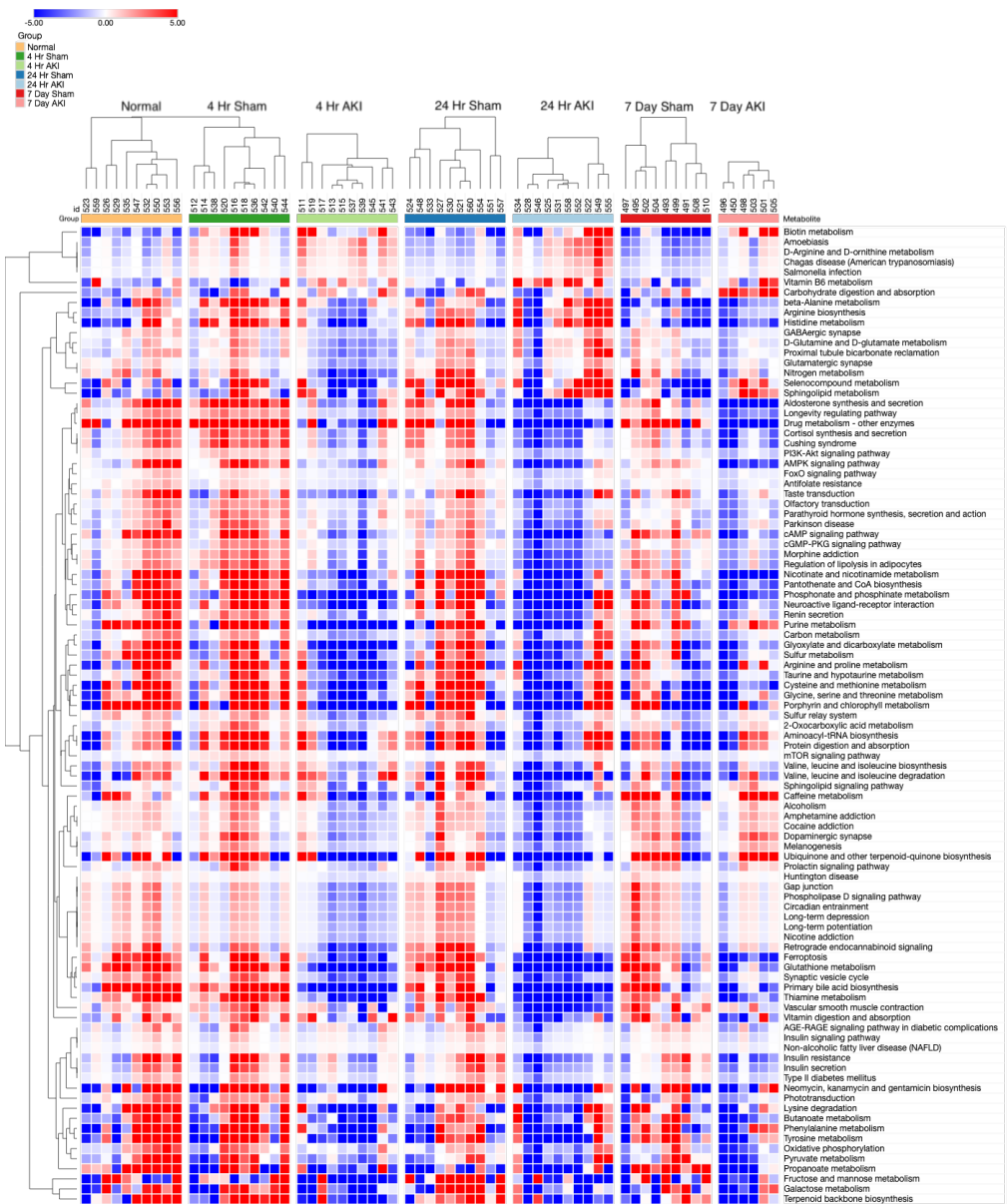


Figure 17: Kidney HCA of PAPi (pearson (n-1) correlation metric with average linkage), red is activity score ($AS > 0$), white is $AS = 0$, blue is $AS < 0$

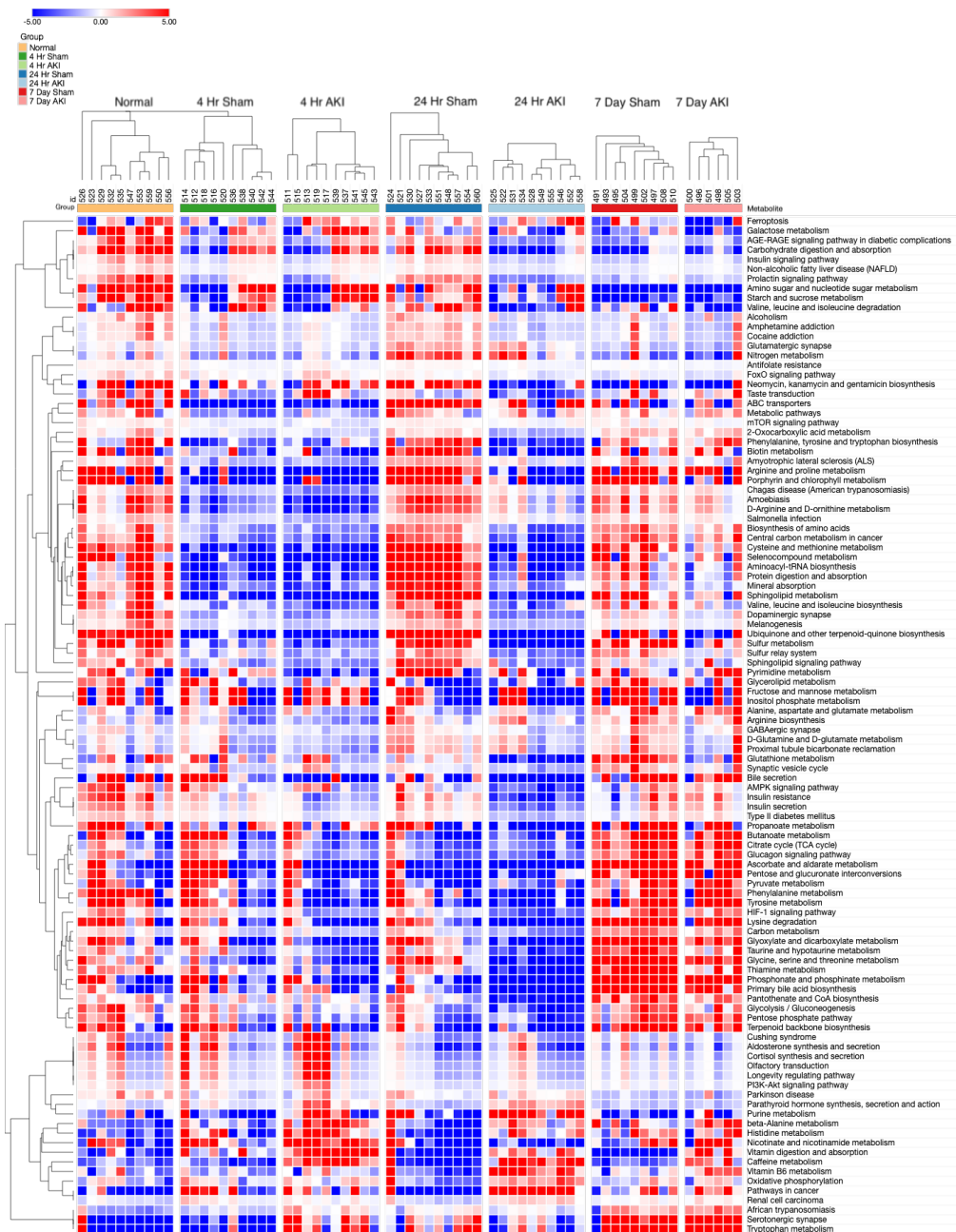


Figure 18: Plasma HCA of PAPi (pearson (n-1) correlation metric with average linkage), red is activity score ($AS > 0$), white is $AS = 0$, blue is $AS < 0$

6.5 Enriched pathways significant to AKI

4 Hours	Lung	Liver	Kidney	Plasma
Heart				
Butanoate metabolism ¹		Nitrogen metabolism ¹		Primary bile acid biosynthesis ¹
Alanine, aspartate and glutamate metabolism ¹		Primary bile acid biosynthesis ¹		Taurine and hypotaurine metabolism ¹
Histidine metabolism ¹		Vitamin B6 metabolism ¹		Pentose phosphate pathway ¹
		Butanoate metabolism ¹		Histidine metabolism ¹
		D-Glutamine and D-glutamate metabolism ¹		Alanine, aspartate and glutamate metabolism ²
		Porphyrin and chlorophyll metabolism ¹		Purine metabolism ²
		Tryptophan metabolism ¹		Cysteine and methionine metabolism ²
		Methane metabolism ¹		Amino sugar and nucleotide sugar metabolism ²
		Glutathione metabolism ¹		Pyrimidine metabolism ²
		Cyanoamino acid metabolism ¹		Aminoacyl-tRNA biosynthesis ²
		Alanine, aspartate and glutamate metabolism ¹		Arginine and proline metabolism ²
		Pentose and glucuronate interconversions ¹		
		Glycine, serine and threonine metabolism ¹		
		Glycerophospholipid metabolism ¹		
		Purine metabolism ¹		
		Cysteine and methionine metabolism ¹		
		Aminoacyl-tRNA biosynthesis ¹		
		Taurine and hypotaurine metabolism ¹		
		Pentose phosphate pathway ¹		
		Sphingolipid metabolism ¹		
		Pyrimidine metabolism ¹		
		Pantothenate and CoA biosynthesis ¹		
		Arginine and proline metabolism ²		
		Histidine metabolism ²		

Table 12: Pathways that were enriched due to the effect of AKI at 4 hours in the heart, lung, liver, kidney, or plasma, 1: Sig2AKI, 2: IiAKI, 3: OppInAKI, 4: NoEfAKI

24 Hours	Lung	Liver	Kidney	Plasma
Heart	Pentose and glucuronate interconversions ¹	Pentose and glucuronate interconversions ¹	Primary bile acid biosynthesis ¹	Primary bile acid biosynthesis ¹
Primary bile acid biosynthesis ¹		Nitrogen metabolism ¹		Nitrogen metabolism ¹
Cyanoamino acid metabolism ¹		Nitrogen metabolism ¹		Phenylalanine metabolism ¹
Phenylalanine metabolism ¹		Vitamin B6 metabolism ¹		Vitamin B6 metabolism ¹
Lysine degradation ¹		Butanoate metabolism ¹		Starch and sucrose metabolism ¹
Phenylalanine, tyrosine and tryptophan biosynthesis ¹		Pyrimidine metabolism ¹		Lysine degradation ¹
Butanoate metabolism ¹		D-Glutamine and D-glutamate metabolism ¹		Amino sugar and nucleotide sugar metabolism ¹
Purine metabolism ¹		Porphyrin and chlorophyll metabolism ¹		Porphyrin and chlorophyll metabolism ¹
Glycine, serine and threonine metabolism ¹		Arginine and proline metabolism ¹		Valine, leucine and isoleucine degradation ¹
Vitamin B6 metabolism ¹		Valine, leucine and isoleucine biosynthesis ¹		Methane metabolism ¹
Lysine biosynthesis ¹		Pentose phosphate pathway ¹		Valine, leucine and isoleucine biosynthesis ¹
Pantothenate and CoA biosynthesis ¹		Glutathione metabolism ¹		Glutathione metabolism ¹
beta-Alanine metabolism ¹		Cyanoamino acid metabolism ¹		Cyanoamino acid metabolism ¹
Porphyrin and chlorophyll metabolism ¹		Sphingolipid metabolism ²		Alanine, aspartate and glutamate metabolism ¹
Glutathione metabolism ¹		Glycine, serine and threonine metabolism ¹		Glycine, serine and threonine metabolism ¹
Methane metabolism ¹		Histidine metabolism ¹		Phenylalanine, tyrosine and tryptophan biosynthesis ¹
Pentose phosphate pathway ¹		Taurine and hypotaurine metabolism ¹		Purine metabolism ¹
Tyrosine metabolism ¹		Pentose phosphate pathway ¹		Histidine metabolism ¹
Nitrogen metabolism ²		Citrate cycle (TCA cycle) ¹		Cysteine and methionine metabolism ¹
Alanine, aspartate and glutamate metabolism ²		Nicotinate and nicotinamide metabolism ¹		Aminoacyl-tRNA biosynthesis ¹
Histidine metabolism ²		Pantothenate and CoA biosynthesis ¹		Pyrimidine or Gluconeogenesis ¹
D-Glutamine and D-glutamate metabolism ²		Arginine and proline metabolism ¹		Taurine and hypotaurine metabolism ¹
Pyrimidine metabolism ²				Pentose phosphate pathway ¹
Aminoacyl-tRNA biosynthesis ²				Tyrosine metabolism ¹
Taurine and hypotaurine metabolism ²				Citrate cycle (TCA cycle) ¹
Arginine and proline metabolism ²				Pyrimidine metabolism ¹
				Galactose metabolism ¹
				Pantothenate and CoA biosynthesis ¹
				Arginine and proline metabolism ¹
				Lysine biosynthesis ¹

Table 13: Pathways that were enriched due to the effect of AKI at 24 hours in the heart, lung, liver, kidney, or plasma, 1: Sig2AKI, 2: IiAKI, 3: OppInAKI, 4: NoEfAKI

7 Days		Liver	Kidney	Plasma
Heart	Lung			
Pentose and glucuronate interconversions ¹		Cyanoamino acid metabolism ¹	Pentose and glucuronate interconversions ¹	Vitamin B6 metabolism ¹
		Glycine, serine and threonine metabolism ¹		Pantothenate and CoA biosynthesis ¹
		Butanoate metabolism ¹		Cysteine and methionine metabolism ¹
		Glycerophospholipid metabolism ¹		
		Cysteine and methionine metabolism ¹		
		Nicotinate and nicotinamide metabolism ¹		
		Vitamin B6 metabolism ¹		
		Pantothenate and CoA biosynthesis ¹		
		Glutathione metabolism ¹		
		Arginine and proline metabolism ¹		
		Starch and sucrose metabolism ¹		
		Valine, leucine and isoleucine biosynthesis ¹		
		beta-Alanine metabolism ¹		
		Tyrosine metabolism ¹		

Table 14: Pathways that were enriched due to the effect of AKI at 7 days in the heart, lung, liver, kidney, or plasma, 1: Sig2AKI, 2: IiAKI, 3: OppInAKI, 4: NoEfAKI

6.6 Box and whisker plots

6.6.1 Amino acids in the heart

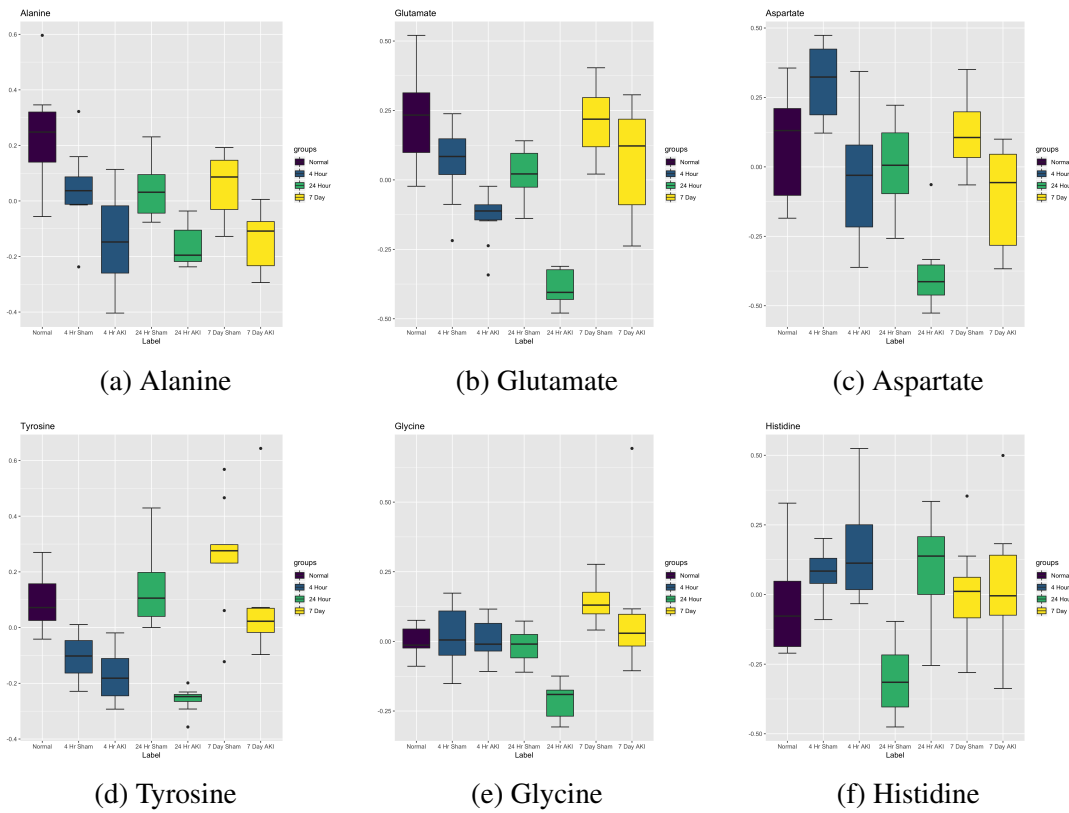


Figure 19: Box and whisker plots of glucogenic amino acids at all time points in the heart

6.6.2 Amino acids in the lung and liver

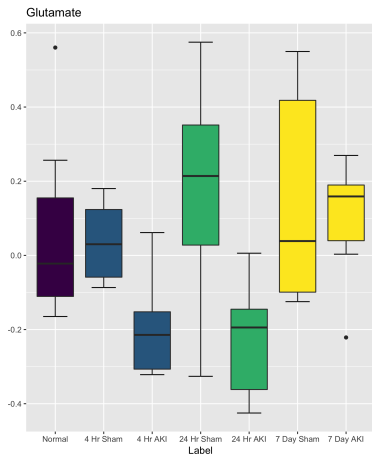


Figure 20: Lung glutamate levels

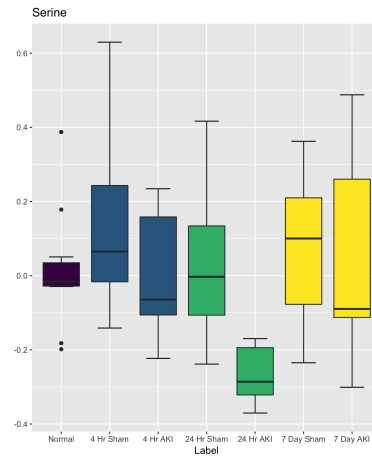


Figure 21: Liver serine levels

6.6.3 Glycolysis/TCA Cycle/Pentose Phosphate Pathway

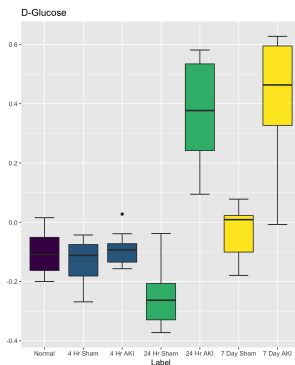


Figure 22: Heart glucose levels

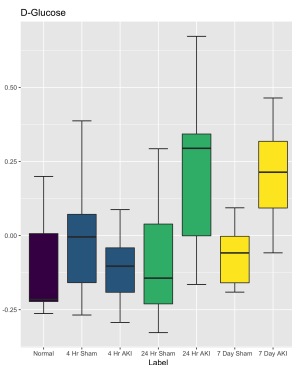


Figure 23: Lung glucose levels

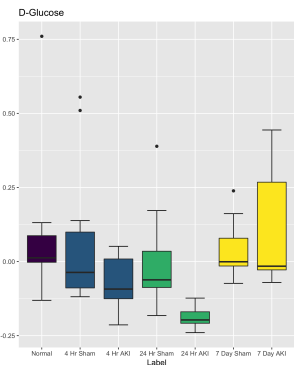


Figure 24: Liver glucose levels

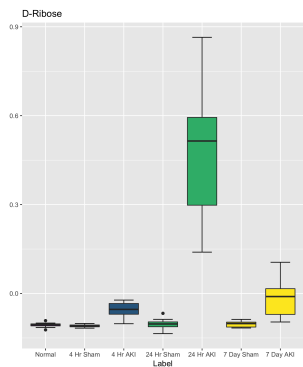


Figure 25: Heart ribose levels

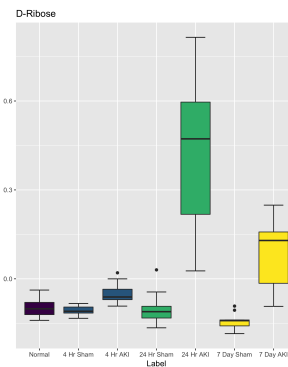


Figure 26: Lung ribose levels

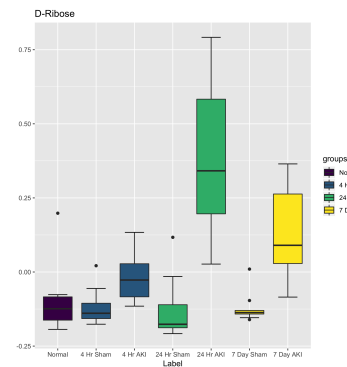


Figure 27: Liver ribose levels

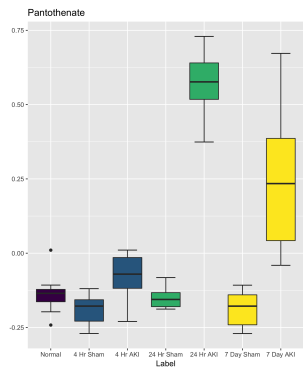


Figure 28: Heart pantothenate levels

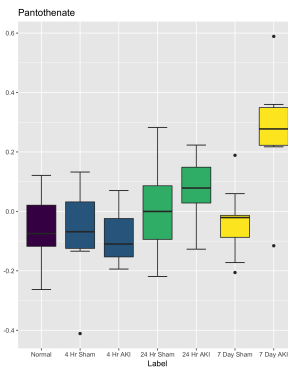


Figure 29: Lung pantothenate levels

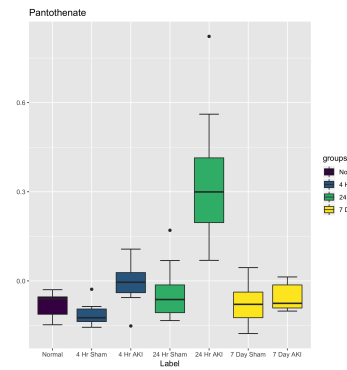


Figure 30: Liver pantothenate levels

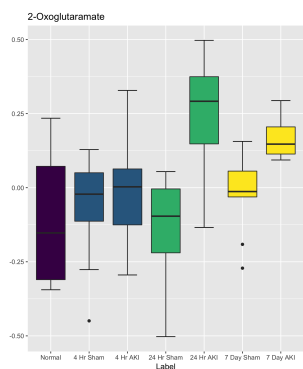
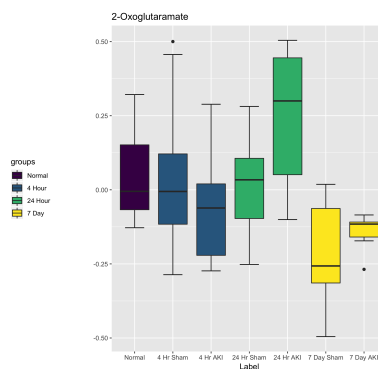


Figure 31: Heart oxoglutaramate levels



2- Figure 32: Lung 2-oxoglutaramate levels

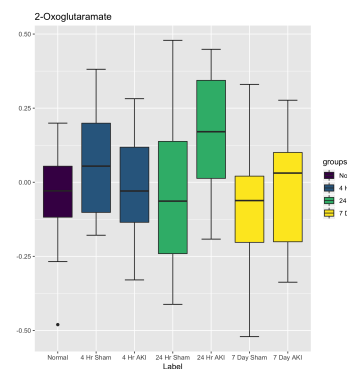
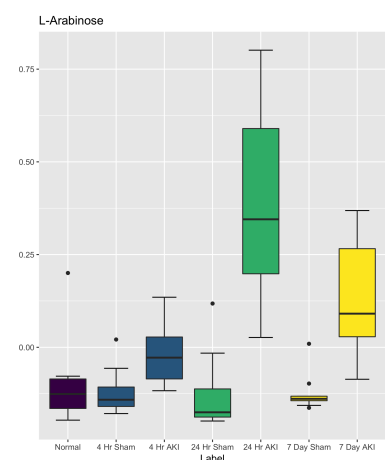
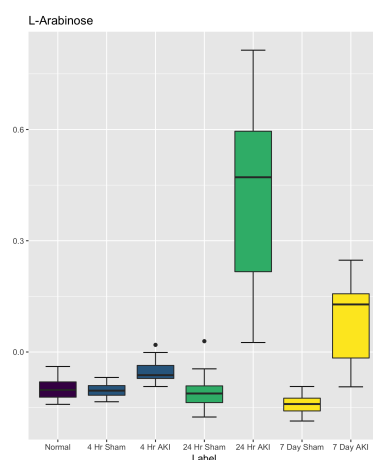
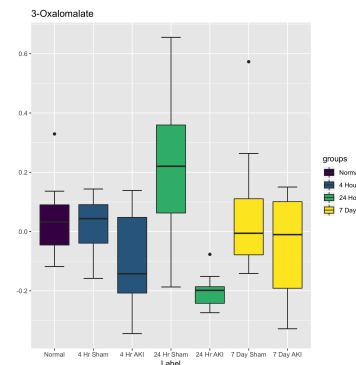
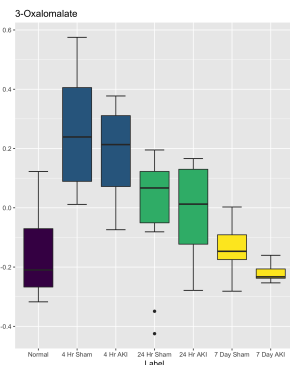
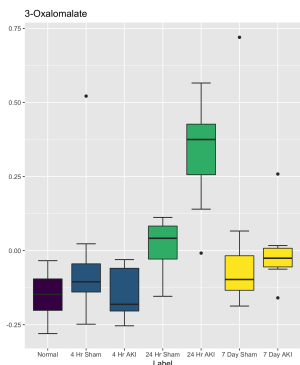


Figure 33: Liver 2-oxoglutaramate levels



6.6.4 Purine and pyrimidine metabolism

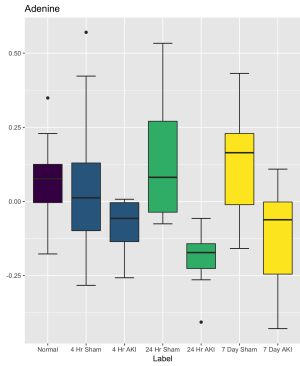


Figure 39: Heart adenine levels

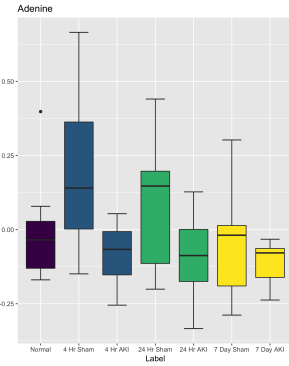


Figure 40: Lung adenine levels

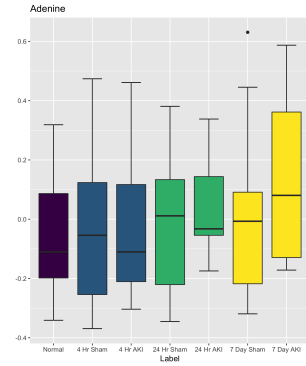


Figure 41: Liver adenine levels

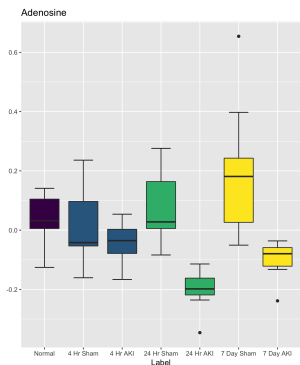


Figure 42: Heart adenosine levels

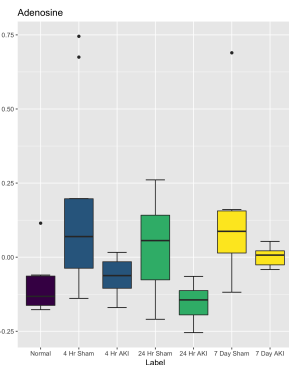


Figure 43: Lung adenosine levels

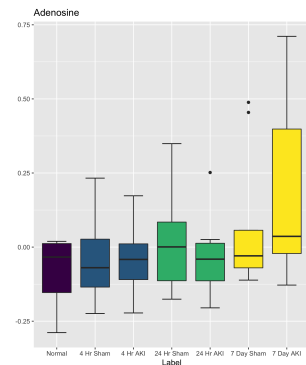


Figure 44: Liver adenosine levels

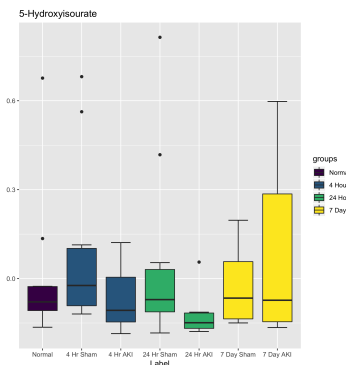
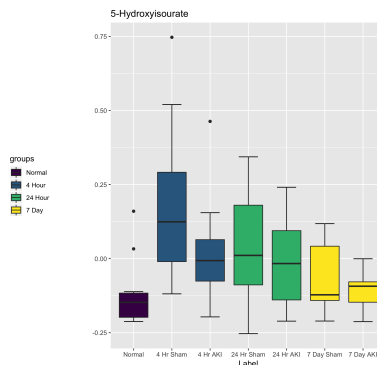
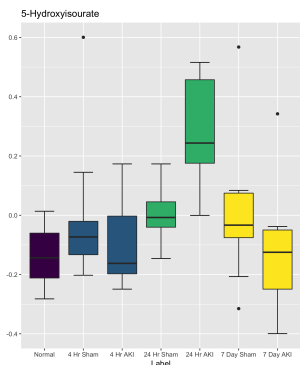


Figure 45: Heart hydroxyisourate levels

Figure 46: Lung hydroxyisourate levels

Figure 47: Liver hydroxyisourate levels

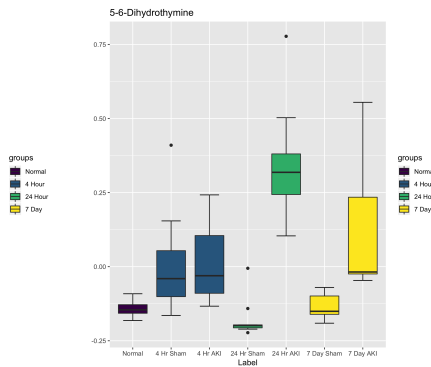
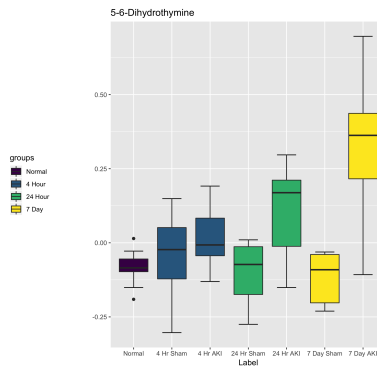
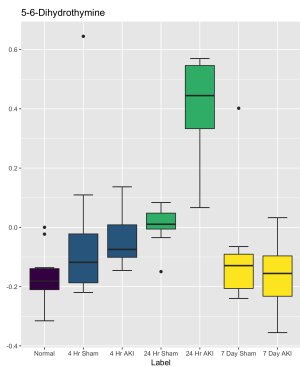


Figure 48: Heart dihydrothymine levels

Figure 49: Lung dihydrothymine levels

Figure 50: Liver dihydrothymine levels

6.6.5 Oxidative stress

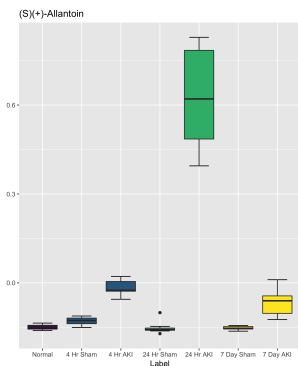


Figure 51: Heart S-allantoin levels

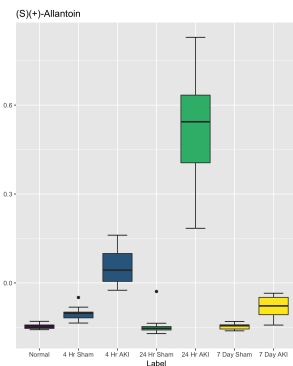


Figure 52: Lung S-allantoin levels

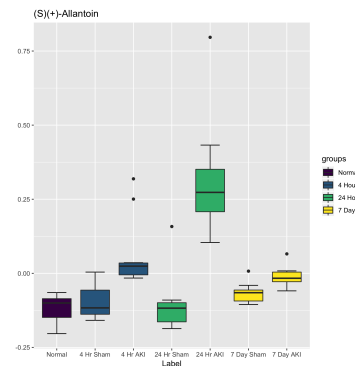


Figure 53: Liver S-allantoin levels

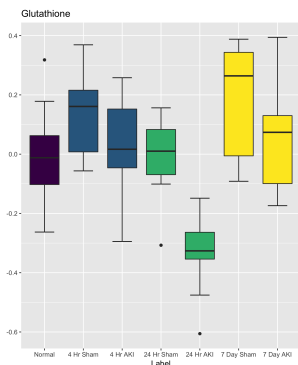


Figure 54: Heart glutathione levels

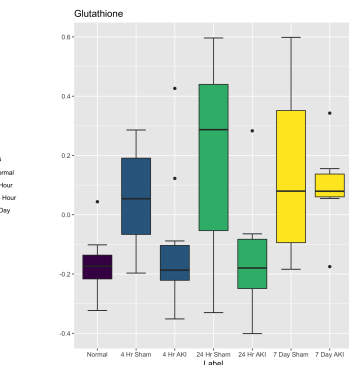


Figure 55: Lung glutathione levels

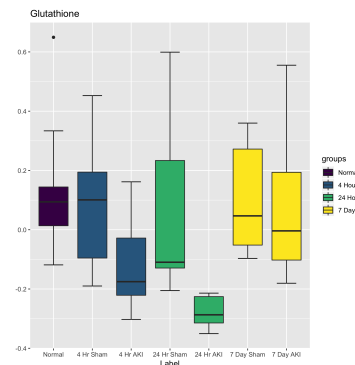


Figure 56: Liver glutathione levels

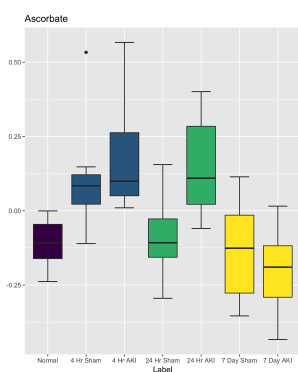


Figure 57: Heart ascorbate levels

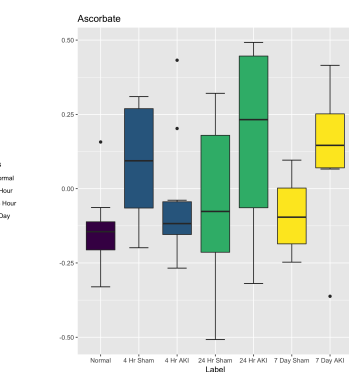


Figure 58: Lung ascorbate levels

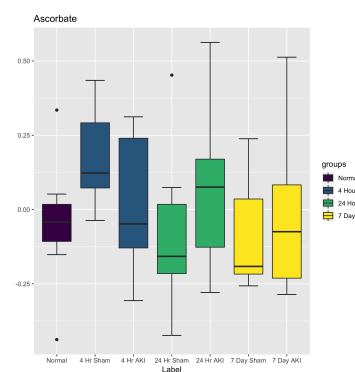


Figure 59: Liver ascorbate levels

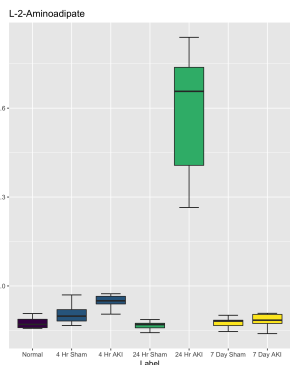


Figure 60: Heart L-2-amino adipate levels

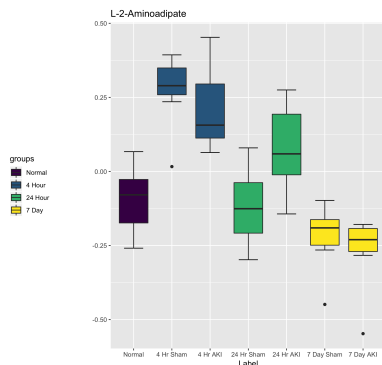


Figure 61: Lung L-2-amino adipate levels

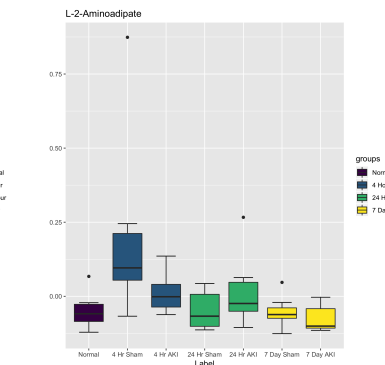


Figure 62: Liver L-2-amino adipate levels

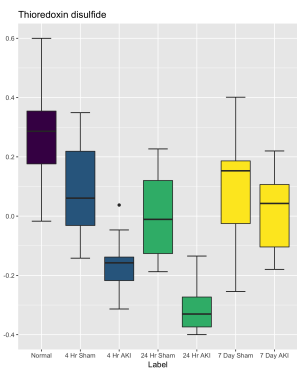


Figure 63: Heart thioredoxin disulfide levels

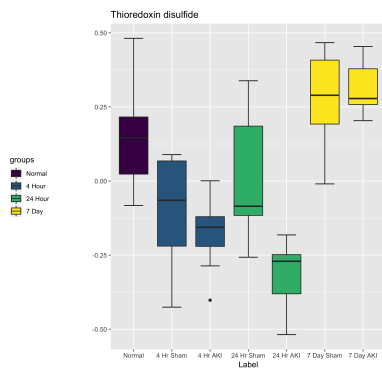


Figure 64: Lung thioredoxin disulfide levels

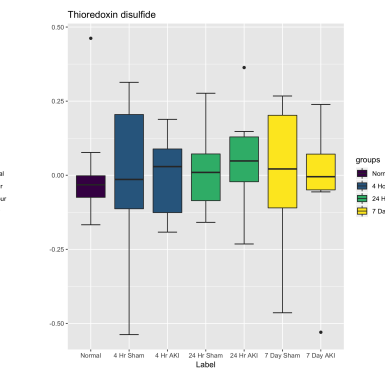


Figure 65: Liver thioredoxin disulfide levels

6.7 Metabolites with the highest cosine similarity metrics in PCA

Heart PC1PC2	PC1PC3	PC2PC3
Pantothenate	(S)(+)-Allantoin	NAD+
(S)(+)-Allantoin	Pantothenate	Malate
L-2-Aminoadipate	L-2-Aminoadipate	D-Erythrose 4-phosphate
cis-Zeatin	cis-Zeatin	D-Glucono-1,5-lactone 6-phosphate
D-Glucose	D-Ribose	ADP
D-Ribose	Aspartate	Fumarate
D-Glucono-1,5-lactone 6-phosphate	Glutamate	Nicotinamide
D-Erythrose 4-phosphate	D-Glucose	5-Oxoproline
Glutamate	5-6-Dihydrothymine	Valine
Aspartate	Phosphoserine	Phosphocreatine
NAD+	Threonate	D-Glucose 6-phosphate
Threonate	Glutathione	D-Ribitol 5-phosphate
5-6-Dihydrothymine	Malate	Arginine
Phosphoserine	Fumarate	Cytidine
Nicotinamide	5-Hydroxyisourate	Ethanolamine phosphate
D-Glucose 6-phosphate	Dethiobiotin	AMP
Phosphocreatine	6-Phospho-D-gluconate	N-Glycoloyl-neuraminate
Valine	Peptide tryptophan	Glutathione disulfide
Pyridoxamine	Thioredoxin disulfide	Lactate
Thioredoxin disulfide	3-Oxalomalate	Inosine
Glutathione	NAD+	Hypoxanthine
Cytidine	N-Carbamyl-L-glutamate	Phosphate
2-Hydroxyglutarate/Citramalate	2-Oxoglutarate	Leucine
Peptide tryptophan	ADP	Dethiobiotin
Lysine	2-Hydroxyglutarate/Citramalate	L-Carnitine

Table 15: Top 25 metabolites with the largest sum of squared cosines between the two principal components in the heart

Lung			
PC1PC2	PC1PC3		PC2PC3
Proline	Glycine		(S)(+)-Allantoin
Malate	Proline		D-Ribose
Glycine	Malate		L-Arabinose
Phosphoserine	Hydroxyacetone phosphate		N-Amidino-L-aspartate
Alanine	Taurine		Creatinine
Hydroxyacetone phosphate	Serine		Thioredoxin disulfide
Methylenediuera	Alanine		Putrescine
Cytidine	Cytidine		2-Oxo-7-methylthioheptanoic acid
Serine	Hypoxanthine		Ethanolamine phosphate
Hypoxanthine	N-Acetylneuraminate		N6-Methyl-L-lysine
N-Acetylneuraminate	D-Glyceraldehyde 3-phosphate/Glycerone phosphate		4-Pyridoxate
cis-p-Coumarate	Pyridoxamine		2,3-Bisphosphoglycerate
D-Glyceraldehyde 3-phosphate/Glycerone phosphate	Threonine		Pyridoxamine
Threonine	5-Oxoproline		Aspartate
Methionine	gamma-L-Glutamyl-D-alanine		O-Propanoylcarnitine
Glutamate	Methionine		L-2-Aminoadipate
gamma-L-Glutamyl-D-alanine	Phosphoserine		D-Glucose
Creatine	Lysine		Homocarnosine
5-Oxoproline	Methylenediuera		2-Hydroxyglutarate/Citramalate
Tyrosine	trans-4-Hydroxy-L-proline		Phosphocreatine
trans-4-Hydroxy-L-proline	3-Sulfino-L-alanine		Maleamate
Taurine	L-Cysteate		2/3-Phospho-D-glycerate
(S)(+)-Allantoin	S-Adenosyl-L-homocysteine		Ascorbate
3-Sulfino-L-alanine	cis-p-Coumarate		Lysine
S-Adenosyl-L-homocysteine	Valine		Glutamate

Table 16: Top 25 metabolites with the largest sum of squared cosines between the two principal components in the lung

Liver		
PC1PC2	PC1PC3	PC2PC3
Sodium glucuronate	Oxaloacetate	2',3'-Cyclic CMP
2',3'-Cyclic CMP	Proline	ADP
Oxaloacetate	5-Hydroxyisourate	L-Arabinose
Proline	Nicotinamide	D-Ribose
alpha-D-Glucosamine 1-phosphate	Glutathione	Phosphocreatine
D-Ribitol 5-phosphate	5-Oxoproline	5,6-Dihydrothymine
Nicotinamide	Glutamine	L-Homocitrulline
6-Phospho-D-gluconate	Mercaptopyruvate	N-Acyl-D-mannosaminolactone
5-Hydroxyisourate	Glycerol 3-phosphate	5-Guanidino-2-oxopentanoate
Glutathione	O-Propanoylcarnitine	L-Citrulline
3D-(3,5/4)-Trihydroxycyclohexane-1,2-dione	6-Phospho-D-gluconate	Methylenediuera
Phosphocreatine	Cys-Gly	Creatine
5-Oxoproline	Histidine	Sodium glucuronate
O-Propanoylcarnitine	Phenylalanine	NAD+
Glutamine	S-Acylglutathione	D-Glyceraldehyde 3-phosphate/Glycerone phosphate
Glycerol 3-phosphate	ADP	Inosine
Histidine	3-Phospho-D-erythronate	Creatinine
L-Cysteate	cis-p-Coumarate	D-Glucono-1,5-lactone 6-phosphate
Mercaptopyruvate	5,10-Methenyltetrahydrofolate	D-Ribitol 5-phosphate
Cys-Gly	NAD+	D-Glucose 6-phosphate
3-Sulfino-L-alanine	Inosine	5-Phospho-alpha-D-ribose 1-diphosphate
5-Guanidino-2-oxopentanoate	Methionine	Pantothenate
S-Acylglutathione	Phosphoserine	Hypoxanthine
N-Acyl-D-mannosaminolactone	Serine	Threonate
cis-p-Coumarate	Thymidine	Pentose phosphates (isobars)

Table 17: Top 25 metabolites with the largest sum of squared cosines between the two principal components in the liver

Kidney PC1PC2	PC1PC3	PC2PC3
Ectoine	Glycine	UDP-N-acetyl-D-glucosamine
Glycine	Poly-gamma-D-glutamate	Decanoic acid (caprate)
Poly-gamma-D-glutamate	Ectoine	UDP-glucose
gamma-L-Glutamyl-L-cysteine	gamma-L-Glutamyl-L-cysteine	Urate
4-Acetamidobutanoate	Adenine	Indole
L-Citrulline	L-Homocysteine	Picolinic acid
N-Amidino-L-aspartate	N-Amidino-L-aspartate	2-Hydroxyglutarate/Citramalate
Pyridoxal	NAD+	N-Acyl-D-aspartate
L-Homocysteine	N-Glycoloyl-neuraminate	Creatine
Adenine	UDP-N-acetyl-D-glucosamine	Xanthine
Decanoic acid (caprate)	Hypoxanthine	Methylenediuera
NAD+	Pyridoxal	Tryptophan
Homomethionine	Cysteine	ADP-D-ribose
N-Carbamyl-L-glutamate	Xanthine	Phenylalanine
N-Glycoloyl-neuraminate	L-Citrulline	Dopamine
Cysteine	Guanidinoacetate	Dehydroascorbate
L-Homocitrulline	N-Carbamyl-L-glutamate	Proline
Guanidinoacetate	UDP-glucose	Diphosphate
Hypoxanthine	4-Acetamidobutanoate	Thymidine
UDP-glucose	L-Carnitine	gamma-L-Glutamylputrescine
5-Oxoproline	Decanoic acid (caprate)	Serine
AMP	Adenosine	3-Methyleneoxindole
2-Hydroxyglutarate/Citramalate	Hydroxyacetone phosphate	Threonine
Creatinine	5-L-Glutamyl-taurine	Phosphate
L-Arabinose	GMP	Alanine

Table 18: Top 25 metabolites with the largest sum of squared cosines between the two principal components in the kidney

Plasma		
PC1PC2	PC1PC3	PC2PC3
Creatinine	Creatinine	Threonine
(5-L-Glutamyl)-peptide	(5-L-Glutamyl)-peptide	Dehydroascorbate
Threonate	Threonate	Arginine
(S)(+)-Allantoin	Hypoxanthine	Oxaloacetate
Hypoxanthine	(S)(+)-Allantoin	2-Oxoglutarate
Ascorbate	Ascorbate	Nicotinamide
5-Guanidino-2-oxopentanoate	Dethiobiotin	5-Oxoproline
Serine	Proline	L-Methionine S-oxide
2/3-Phospho-D-glycerate	D-Ribose	Proline
beta-D-Glucuronoside	5-Guanidino-2-oxopentanoate	Methionine
N-Acyl-D-aspartate	Serine	2-Hydroxyglutarate/Citramalate
Dethiobiotin	Arginine	Citrate
L-Adrenaline	beta-D-Glucuronoside	Guanine
D-Ribose	D-Rhamnose	S-Glutathionyl-L-cysteine
Methionine	L-Adrenaline	2/3-Phospho-D-glycerate
2-Oxoglutarate	Alanine	2-Methyleneglutarate
2-Deoxy-alpha-D-glucoside	N-Acyl-D-aspartate	Pyruvate
Cystine	O-Propanoylcarnitine	Glutamine
Phosphate	Nicotinamide	Alanine
Oxaloacetate	2-Deoxy-alpha-D-glucoside	D-Glucose
Methylenediuera	Methylenediuera	Serine
Guanine	L-Homocitrulline	D-Ribose 5-diphosphate
4-Pyridoxate	4-Pyridoxate	Malate
D-Rhamnose	Creatine	N-Acetylornithine
Malate	Homomethionine	Thymine

Table 19: Top 25 metabolites with the largest sum of squared cosines between the two principal components in the plasma

6.8 Metabolites with the highest PLS-DA weights

Heart		24 Hr AKI		4 Hr AKI		4 Hr Sham		7 Day AKI		7 Day Sham		Normal	
(S)-4-hydroxybutyrate	Ornithine	Metformine	Metformine	S-Glycathionyl-L-cysteine	N-Glycathionyl-neuraminate	N-Glycathionyl-neuraminate	N-Glycathionyl-neuraminate	L-leucine	Leucine	Pyridoxamine	Pyridoxamine	Ornithine	Ornithine
Phenylalanine	Taurine			N6-Methyl-L-lysine	Methionine			4-Aminobenzoate	Methionine				
L-2-Aminoadipate	N6-Methyl-L-lysine			5-Oxoproline	Methionine	5-Oxoprolines		S-Glycathionyl-L-cysteine	Catechin				
cis-Zeatin	Histidine			Ornithine	Ethanolamine phosphate	4-Aminobenzoate	Spermidine	Thioredoxin disulfide					
D-Ribose	5-Oxoproline			Succinate	N-Glycathionyl-neuraminate	Serine	Ethanolamine phosphate	4-Pyridoxate					
Glutamate	Catechin			Arginine	Succinate	Valine	Pyridoxamine	N6-Methyl-L-lysine					
Alanine	Quinolinicacid			Serine	Aspartate	Ethanolamine phosphate	Pyridoxamine	Ornithine					
Phosphoserine	Ornithine			S-Glycathionyl-L-cysteine	Pyruvate	L-Carnitine	Valine	Serotonin					
5,6-Dihydroxydihydronicotinic acid	Proline			Aspartate	Ethanolamine phosphate	L-Carnitine							
D-Glucose	Lactate			N-Glycathionyl-neuraminate	Cystathione	Lysine	Catechin						
Threonine	L-Citrulline			Spermidine	Diphosphoinositide	D-Erythrose 4-phosphate	Tricarboxylic						
Thioredoxin disulfide	Serotonin			Ethanolamine phosphate	Ascorbate	Phosphocreatine	Pyridoxamine 5'-phosphate						
Glutathione				Serotonin	Cys-Gly	Glycerol 3-phosphate	Pyridoxamine 5'-phosphate						
Pyroglutamyl tryptophan	trans-4-Hydroxy-L-proline			Histidine	Nicotinamide	D-Glutamyl-1-lactone 6-phosphate	Pyridoxamine						
3-Oxalosuccinate	Alanine			Pyruvate	Spermidine	Nicotinamide	Pyridoxamine						
Tyrosine	D-Glyceraldehyde 3-phosphate/Glycerone phosphate			Tyrosine	Ornithine	Arginine	Arginine						
Pyridoxamine	4-Pyridoxate			4-Aminobenzoate	Oxalosuccinate	L-Citrulline	2-Oxo-7-methylthioheptanoic acid						
2-Oxoglutaramate	3-Sulfino-L-alanine			L-Cysteate	Phosphatidylserine	NAD+	L-Adrenaline						
2-Oxo-7-methylthioheptanoic acid				Dethiobiotin	O-Palmitoylcarnitine	2-Oxo-7-methylthioheptanoic acid	Aspartate						
Lysine	4-Aminobenzoate			NAD+	Tryptophan	Histidine	Ornithine						
3-Sulfino-L-alanine	Succinate			trans-4-Hydroxy-L-proline	trans-4-Hydroxy-L-proline	L-Octanoylcarnitine	N-Aminido-L-aspartate						
5-Hydroxyisourate	Phosphoserine			Cystathione	L-Cysteate	L-Adrenalin	2-Oxopropionate						
S-Glutathionyl-L-cysteine	Pyridoxamine			D-Glucose	1-O-Galloyl-beta-D-glucose	Cytidine	Phosphocreatine						
2-Hydroxyglutarate/Citramalate	Dethiobiotin			Oxalosuccinate	Thioredoxin disulfide	UMP	(S,L-Glutamyl)-peptide						
6-Phospho-D-glucuronate	Valine			Ascorbate	2-Oxo-7-methylthioheptanoic acid	Tyrosine	trans-4-Hydroxy-L-proline	D-Fructose 1,6-bisphosphate					

Table 20: Top 25 metabolites with the largest weights for the PLS-DA model prediction for each sample group in the heart

Lung		24 Hr AKI		4 Hr AKI		4 Hr Sham		7 Day AKI		7 Day Sham		Normal	
(S)(+)-Allantoin	O-Butanoylcarnitine	Homocarnosine	Homocarnosine	4-Aminobenzoate	4-Aminobenzoate	4-Aminobenzoate	4-Aminobenzoate	4-Aminobenzoate	4-Aminobenzoate	O-Butanoylcarnitine			
Putrescine	Glutathione	2-Hydroxyglutarate/Citramalate	2-Hydroxyglutarate/Citramalate	Maleamate	Maleamate	Maleamate	Maleamate	5,6-Dihydroxydihydronicotinic acid	5,6-Dihydroxydihydronicotinic acid	Homocarnosine	Glutathione		
Thioredoxin disulfide	Cys-Gly	Ethanolamine phosphate	Phosphocreatine	Ornithine	Ornithine	Ornithine	Ornithine	Homocarnosine	Homocarnosine	Ethanolamine phosphate	Cysteine		
Creatinine	Homocarnosine	4-Aminobenzoate	Tryptophan	L-Carnitine	2,3-Bisphosphoglycerate	2,3-Bisphosphoglycerate	2,3-Bisphosphoglycerate	2,3-Bisphosphoglycerate	2,3-Bisphosphoglycerate	Cys-Gly			
D-Ribose	Ethanolamine phosphate			Maleamate	4-Aminobenzoate	Ethanolamine phosphate	Ethanolamine phosphate	N6-Methyl-L-lysine	N6-Methyl-L-lysine	Thioredoxin disulfide	Thioredoxin disulfide		
L-Arabinitol	Cysteine			2-Oxoglutarate	4-Aminobenzoate	2,3-Phospho-D-glycerate	2,3-Phospho-D-glycerate	Pantothenate	Pantothenate	Tryptophan	Tryptophan		
N-Aminido-L-aspartate	Penrose phosphates (isobars)			5-Oxopropionate	5-O-Propionylcarnitine	5-O-Propionylcarnitine	5-O-Propionylcarnitine	5-O-Propionylcarnitine	5-O-Propionylcarnitine	Penrose phosphates (isobars)	Penrose phosphates (isobars)		
Homocarnosine	Uracil			5-O-Propionylcarnitine	5-O-Propionylcarnitine	5-O-Propionylcarnitine	5-O-Propionylcarnitine	5-O-Propionylcarnitine	5-O-Propionylcarnitine	Uracil	Uracil		
N6-Methyl-L-lysine	2,4,6-tri-7-methylthioheptanoic acid			5-O-Propionylcarnitine	5-O-Propionylcarnitine	5-O-Propionylcarnitine	5-O-Propionylcarnitine	5-O-Propionylcarnitine	5-O-Propionylcarnitine	2,3-Bisphosphoglycerate	2,3-Bisphosphoglycerate		
Phosphoserine	2-Oxoglutarate			5-O-Propionylcarnitine	5-O-Propionylcarnitine	5-O-Propionylcarnitine	5-O-Propionylcarnitine	5-O-Propionylcarnitine	5-O-Propionylcarnitine	2-Oxoglutarate	2-Oxoglutarate		
4-Pyridoxate	D-Fructose 6-phosphate			Ornithine	2-Oxoglutarate	Maleamate	Maleamate	(S)(+)-Allantoin	(S)(+)-Allantoin	Maleamate	Maleamate		
O-Propionylcarnitine	1-Octanoylcarnitine			O-Propionylcarnitine	2-Oxoglutarate	D-Glucose	2,3-Bisphosphoglycerate	2,3-Bisphosphoglycerate	2,3-Bisphosphoglycerate	1-Octanoylcarnitine	1-Octanoylcarnitine		
D-Glucose	2-Hydroxyglutarate/Citramalate			Phosphocreatine	Ethanolamine phosphate	2-Oxoglutarate	2-Oxoglutarate	2-Oxoglutarate	2-Oxoglutarate	D-Glucose	D-Glucose		
Glutamate	Spermine			3-Phosphonoxypropyruvate	Adenosine	Adenosine	Thioredoxin disulfide	2-Oxoglutarate	2-Oxoglutarate	O-Butanoylcarnitine	2-Oxoglutarate		
Asparagine	L-2-Aminoadipate			Succinate	Valine	D-Glucose 6-phosphate	D-Glucose 6-phosphate	D-Glucose 6-phosphate	D-Glucose 6-phosphate	O-Butanoylcarnitine	O-Butanoylcarnitine		
2-Oxoglutaramate	D-Glyceraldehyde 3-phosphate/Glycerone phosphate			2,3-Phospho-D-glycerate	3-Phosphonoxypropyruvate	Tryptophan	Tryptophan	Tryptophan	Tryptophan	O-Butanoylcarnitine	O-Butanoylcarnitine		
Aspartate	Ornithine			2-Oxo-7-methylthioheptanoic acid	(S)(+)-Allantoin	Uracil	2-Oxo-7-methylthioheptanoic acid	2-Oxo-7-methylthioheptanoic acid	2-Oxo-7-methylthioheptanoic acid	Ornithine	Ornithine		
L-Adrenaline	O-Propionylcarnitine			Spermine	L-Adrenalin	Aspartate	Aspartate	Aspartate	Aspartate	Putrescine	Putrescine		
L-2-Aminoadipate	2,3-Bisphosphoglycerate			Adenosine	5,6-Dihydroxydihydronicotinic acid	D-Glucose	2,3-Bisphosphoglycerate	2,3-Bisphosphoglycerate	2,3-Bisphosphoglycerate	Spermine	Spermine		
L-Carnitine	Tryptophan			Peptidyl-tryptophan	5-O-Acetyluraminate	2-Oxoglutarate	2-Oxoglutarate	2-Oxoglutarate	2-Oxoglutarate	2,3-Bisphosphoglycerate	2,3-Bisphosphoglycerate		
Ascorbate	Maleamate			O-Butanoylcarnitine	Tryptophan	AMP	AMP	AMP	AMP	2,3-Bisphosphoglycerate	2,3-Bisphosphoglycerate		
Methylenediox urea	Serine			O-Butanoylcarnitine	N6-Methyl-L-lysine	N-Carbamyl-L-glutamate	N-Carbamyl-L-glutamate	N-Carbamyl-L-glutamate	N-Carbamyl-L-glutamate	D-Fructose 6-phosphate	D-Fructose 6-phosphate		
Fumarate	D-Ribitol 5-phosphate			L-Citrulline	N6-Methyl-L-lysine	L-2-Aminoadipate	O-Propionylcarnitine	O-Propionylcarnitine	O-Propionylcarnitine	D-Ribitol 5-phosphate	D-Ribitol 5-phosphate		
Creatine	Xanthine			4-Pyridoxate	Pyridoxamine	L-Octanoylcarnitine	AMP	AMP	AMP	Serine	Serine		
2,3-Bisphosphoglycerate	Indole-3-acetaldehyde			Pantothenate	Glycine	3-Sulfino-L-alanine	Fumarate	Fumarate	Fumarate	D-Glucose 6-phosphate	D-Glucose 6-phosphate		

Table 21: Top 25 metabolites with the largest weights for the PLS-DA model prediction for each sample group in the lung

Liver	24 Hr AKI	24 Hr Sham	4 Hr AKI	4 Hr Sham	7 Day AKI	7 Day Sham	Normal
2'-3'-Cyclic CMP	2'-3'-Phospho-D-glycerate	Dopamine	N-Glycoloyl-neuraminate	2'-3'-Phospho-D-glycerate	Dopamine	Dopamine	Dopamine
Sodium glucuronate	Aspartate	N-Glycolyl-neuraminate	Lysine	Dehydroascorbate	Dehydroascorbate	Dehydroascorbate	Dehydroascorbate
Phosphocreatine	ADP	Valine	Pyridoxamine	Pyridoxamine	2-Oxoglutarate	Tryptophan	Tryptophan
D-Ribitol 5-phosphate	Dopamine	Malate	2'-3'-Phospho-D-glycerate	4-Aminobenzoate	L-Carnitine	Pentose phosphates (isobars)	Pentose phosphates (isobars)
alpha-D-Glucosamine 1-phosphate	Pyridoxamine	Pyridoxamine	2-Oxo-7-methylthioheptanoic acid	2-Aminobenzoate	4-Aminobenzoate	Glutathione	Glutathione
L-Arabinoose	Pentose phosphates (isobars)	Lysine	S-Glutathionyl-L-cysteine	Lysine	Lysine	D-Fructose 1,6-bisphosphate	D-Fructose 1,6-bisphosphate
D-Ribose	S-Glutathionyl-L-cysteine	2-Oxo-7-methylthioheptanoic acid	Valine	Inosine	Hypoxanthine	5-Phospho-D-glycerate	5-Phospho-D-glycerate
N-(acyl)D-mannosaminolactone	N-Acetylneuraminate	S-Glutathionyl-L-cysteine	2'-3'-Phospho-D-glycerate	2'-Acylglutathione	Threonate	D-Fructose	D-Fructose
L-Cysteine	S-Acylglutathione	Aspartate	S-Acylglutathione	Sparsidine	Insatine	Hypotaurine	Hypotaurine
Methionenolurea	Dehydroascorbate	Cysteine	Dopamine	UMP	N6-Methyl-L-lysine	Cys-Gly	Cys-Gly
3D-(3,5')-Trihydroxycyclohexane-1,2-dione	3-Oxalomalate	Asparagine	2-Oxogutarate	Tripeptide	Pyridoxamine	Tripeptide	Tripeptide
Creatine	Tryptophan	NAD+	Aspartate	N6-Methyl-L-lysine	AMP	Malate	Malate
5-Guanidino-2-oxopentanate	NAD+	ADP	Hypotaurine	ADP	O-Propanoylcarnitine	Glutamate	Glutamate
Creatinine	D-Glucono-1,5-lactone 6-phosphate	Hypotaurine	2-Oxoglutarate	Diphosphate	D-Ribitol 5-phosphate	D-Ribitol 5-phosphate	D-Ribitol 5-phosphate
5,6-Dihydroxyimine	L-Glutamate	cis-p-Cumarate	Threonine	Triglutamate	Asparagine	Asparagine	Asparagine
L-Homocysteine	S-Acetylneuraminate	S-Acylglutathione	Aspartagine	Threonate	Xanthine	L-Carnitine	L-Carnitine
N-Glycolyl-neuraminate	2-Oxo-7-methylthioheptanoic acid	Glutamate	Dihydroxyacetone	D-Glucono-1,5-lactone 6-phosphate	6-Phospho-D-glucosidase	Aspartate	Aspartate
6-Phospho-D-gluconate	3-Phosphoglycerate	trans-4-Hydroxy-L-proline	L-2-Aminoadipate	6-Phospho-D-glucosidase	2-Oxo-7-methylthioheptanoic acid	Cysteate	Cysteate
Pantothenate	S-Adenosyl-L-homocysteine	Tyrosine	cis-p-Cumarate	Diphosphate	S-Glutathionyl-L-cysteine	ADP	ADP
(S)(+)-Allantoate	2,3-Bisphosphoglycerate	Cytidine	Inosine	Succinyl sulfathiazole	2-Oxoglutarate	Valine	Valine
3-Phosphoglycerate	Succinyl sulfathiazole	3-Oxalomalate	Triaicanthine	Triaicanthine	L-2-Aminoadipate	N-Acetyl-L-citrulline	N-Acetyl-L-citrulline
5-Phospho-alpha-D-ribose 1-diphosphate	Inosine	2-Oxoglutarate	Hypotaurine	Pentose phosphates (isobars)	Spermidine	Methionine	Methionine
Glutathione	D-Malate	Dimethylglycine	Tyrosine	S-Glutathionyl-L-cysteine	S-Adenosyl-L-homocysteine	Uracil	Uracil
D-Glucose 6-phosphate	Fumarate	Dehydroascorbate	Dehydroascorbate	N-Glycolyl-neuraminate	S-Guanidino-2-oxopentanate	Triacanthine	Adenosine
N-Acetyl-L-citrulline	Fumarate	Hypoxanthine	3-Oxalomalate	3-Phosphoinoxyruvate			

Table 22: Top 25 metabolites with the largest weights for the PLS-DA model prediction for each sample group in the liver

Kidney	24 Hr AKI	24 Hr Sham	4 Hr AKI	4 Hr Sham	7 Day AKI	7 Day Sham	Normal
3-Oxomalate	Sorbitol	Homocysteine	L-Gamma-Glutamyl-L-hypoglycin	Arginine	L-Gamma-Glutamyl-L-hypoglycin	L-Gamma-Glutamyl-L-hypoglycin	
5-Hydroxyisourate	N-Glycolyl-neuraminate	Carnosine	Creatine	Creatine	Creatine	Succinate	
Carnosine	L-gamma-Glutamyl-hypoglycin	3-Oxomalate	L-Adrenaline	Methyleneedurea	Methyleneedurea	L-Adrenaline	L-Adrenaline
Homocarnosine	6-Phospho-D-gluconate	Asparagine	Methyleneedurea	Homocarnosine	L-Adrenaline	Creatine	Creatine
5,6-Dihydroxyimine	2-Oxoglutarate	5-Hydroxyisourate	Succinate	Carnosine	Succinate	Hydroxyacetone phosphate	Hydroxyacetone phosphate
(S,L)-Glutamyl-L-glutamine	Serine	5,6-Dihydroxyimine	Asparagine	Dopamine	Asparagine	5-Guanidino-2-oxopentanate	5-Guanidino-2-oxopentanate
N-Succinyl-L-citrulline	UDP-N-acetyl-D-glucosamine	Taurine	Sorbitol	Anthranilate	Sorbitol	L-Carnitine	L-Carnitine
Asparagine	gamma-Glutamyl-gamma-aminobutyrate	Methylenedurea	Peptide tryptophan	4-Aminobenzoate	gamma-Glutamyl-gamma-aminobutyrate	IMP	
N-Amidino-L-aspartate	gamma-Glutamyl-gamma-aminobutyrate	Creatine	gamma-Glutamyl-gamma-aminobutyrate	D-Ribitol 5-phosphate	Leucine	Methylenedurea	Methylenedurea
Methylenedurea	Alanine	Methylenedurea	Peptide tryptophan	Panthothenate	6-Aminohexanoate	Peptide tryptophan	Peptide tryptophan
N-Amidino-L-aspartate	gamma-Glutamyl-gamma-aminobutyrate	2-Methylegulutarate	Leucine	Thymidine	NAD+	5-Guanidino-2-oxopentanate	5-Guanidino-2-oxopentanate
Creatine	alanine	N-Succinyl-L-citrulline	6-Aminohexanoate	N-Acetylneuraminate	Histidine	Hydroxyacetone phosphate	Hydroxyacetone phosphate
S-Guanidino-2-oxopentanate	valine	5-Guanidino-2-oxopentanate	Serine	N-Acetylneuraminate	Peptide tryptophan	2-Dioxo-alpha-D-glucoside	2-Dioxo-alpha-D-glucoside
Taurine	butyromoyl-carnitine	Lactate	Glutamine	Malate	Citrurate	Citrurate	Citrurate
Phosphocreatine	Guanine	Glutamine	Hydroxyacetone phosphate	N-Acetylomithine	gamma-L-Glutamyl-D-alanine	2-Dihydro-3-deoxy-D-glucarate	2-Dihydro-3-deoxy-D-glucarate
N-Carbamyl-L-glutamate	Lactate	Cytidine	Alanine	Phosphoserine	Serine	Guanidinoacetate	Guanidinoacetate
Cytidine	Poly-gamma-D-glutamate	2-Oxoglutamate	Alanine	Urate	Guanine	gamma-L-Glutamyl-L-cysteine	gamma-L-Glutamyl-L-cysteine
N-Acetylneuraminate	propionyl-carnitine	2-Deoxy-alpha-D-glucoside	gamma-L-Glutamyl-D-alanine	L-gamma-Glutamyl-L-hypoglycin	N-Acimido-L-aspartate	Glycogen sulfate	Glycogen sulfate
Homometheione	Creatine	Pantothenate	D-Rhamnose	Acetylcholine	Alanine	Homometheione	Homometheione
2-Deoxy-alpha-D-glucoside	Guanosine	S-Formylglutathione	Thymidine	Aspartate	Aspartate	L-Homocysteine	L-Homocysteine
Hydroxyacetone phosphate		D-Glucose 6-phosphate	Guanine	butyroyl-carnitine	propionyl-carnitine	gamma-L-Glutamyl-D-alanine	gamma-L-Glutamyl-D-alanine
2-Methyleneglutamate		Phosphocreatine		butyroyl-carnitine	6-Phospho-D-glucosidase	NAD+	NAD+
Sulfite 3-phosphate		Succinate		inositol	butyroyl-carnitine	Exoate	Exoate
Glutamine	D-Ribonose	S-Acylglutathione	Decarboxy acid (caprate)	Taurine	butyroyl-carnitine	Dimethylglycine	5-Oxoproline
S-Formylglutathione	Methylenedurea	Hydroxyacetone phosphate	Shikimate 3-phosphate	Cysteine	Shikimate 3-phosphate	Choline	
D-glucono-1,5-lactone	Leucine	UMP	Aspartate	Cysteine			

Table 23: Top 25 metabolites with the largest weights for the PLS-DA model prediction for each sample group in the kidney

Plasma	24 Hr AKI	24 Hr Sham	4 Hr AKI	4 Hr Sham	7 Day AKI	7 Day Sham	Normal
Cysteine	Tryptophan	Nicotinamide	Cytidine	Cytidine	Cytidine	Cytidine	Tryptophan
(S,L-Glutamyl)-peptide	Guanosine	Cytidine	Nicotinamide	4-Aminobenzoate	4-Aminobenzoate	S-Carbonyl sulfathiazole	S-Carbonyl sulfathiazole
(Sv+) Allantoin	Succinyl sulfathiazole	Tripeptide	Tripeptide	Pyridoxal	Pyridoxal	N-Methyl-L-histidine phosphate	N-Methyl-L-histidine phosphate
Theanine	Serine	Tripeptide	4-Aminobenzoate	Threonine	N6-Methyl-L-lysine	2-Hydroxyglutarate/Citramalate	2-Hydroxyglutarate/Citramalate
L-Adrenaline	5-Oxoproline	2-Methylglutamate	Triacanthine	Threonine	Threonine	Peptide tryptophan	Peptide tryptophan
Hypoxanthine	2-Hydroxyglutarate/Citramalate	N-Acetylornithine	2-Oxoglutarate	3-Sulfocatechol	Purine	Serine	Serine
Ascorbate	D-Ribose 5-diphosphate	2-Hydroxyglutarate/Citramalate	N-Acetylornithine	Tripeptide	5-6-Dihydroxyamine	N6-Methyl-L-lysine	N6-Methyl-L-lysine
5-Guaidino-2-oxopentanoate	Peptide tryptophan	L-2-Aminoadipate	2-Methylglutamate	Arginine	(S,L-Glutamyl)-L-glutamine	Glutamine	Glutamine
4-Pyridoxate	Malate	2-Oxoglutarate	N6-Methyl-L-lysine	Arginine	5-6-Dihydroxyamine	L-2-Aminoadipate	Malate
beta-D-Glucuronoside	(S,L-Glutamyl)-L-glutamine	Arginine	5-6-Dihydroxyamine	Dehydroascorbate	L-Adrenaline	Malate	Malate
L-Carnitine	N-Methylethanolamine phosphate	D-Glucose	Dehydroascorbate	Purine	2-Oxoglutarate	Sedoheptulose 1-phosphate	Sedoheptulose 1-phosphate
N-Acyl-D-aspartate	N6-Methyl-L-lysine	4-Aminobenzoate	2-Hydroxyglutarate/Citramalate	(S,L-Glutamyl)-L-glutamine	Glycine	D-Glucose	D-Glucose
2-Dexoy-alpha-D-glucoside	D-Glucose	Tryptophan	2-Hydroxyglutarate/Citramalate	D-Glucose	D-Glucose	(S,L-Glutamyl)-L-glutamine	(S,L-Glutamyl)-L-glutamine
Uracil	Aspartate	Aspartate	Aspartate	Dehydroascorbate	Dehydroascorbate	D-Glucose 5-diphosphate	D-Glucose 5-diphosphate
O-Propanoylcarnitine	Nicotinamide	Aspartate	Aspartate	N-Acetylmethionine	5-Oxoproline	Nicotinamide	Nicotinamide
Xanthine	Phenylalanine	beta-D-Glucuronoside	Dehydroascorbate	N-Acetylmethionine	N-Acetylmethionine	Cytidine	Cytidine
D-Ribose	L-2-Aminoadipate	5-Guaidino-2-oxopentanoate	Thymine	L-Citrulline	2-Oxoglutarate	Phenylalanine	Phenylalanine
Serine	Methionine	N6-Methyl-L-lysine	L-Citrulline	N6-Methyl-L-lysine	L-Citrulline	Asparagine	Asparagine
Homomethionine	2-Methylene glutamate	Glutathione disulfide	Aspartate	Arginine	Urate	2-Methylene glutamate	2-Methylene glutamate
Methylenedurea	Sedoheptulose 1-phosphate	L-Carnitine	L-Carnitine	L-Selenomethionine	Pyruvate	Phosphoserine	Phosphoserine
Dethiobiotin	N-Acetylornithine	L-Selenomethionine	Glutamine	Pyruvate	Cysteine	L-Selenomethionine	L-Selenomethionine
Creatine	L-Citrulline	Xanthine	D-Glucose	Urate	Cysteine	N-Acetylornithine	N-Acetylornithine
D-Rhamnose	Oxaloacetate	5-6-Dihydroxyamine	Threonine	Thymine	Mannitol	L-Citrulline	L-Citrulline
gamma-L-Glutamyl-D-alanine	Asparagine	N-Methylethanolamine phosphate	Glutathione disulfide	N-Methylethanolamine phosphate	D-Glyceraldehyde 3-phosphate/Glycerone phosphate	Guanine	Guanine
Cytidine	Cytidine	Thymine	L-Adrenaline	S-Glutathionyl-L-cysteine	S-Glutathionyl-L-cysteine		

Table 24: Top 25 metabolites with the largest weights for the PLS-DA model prediction for each sample group in the plasma